nature microbiology

ARTICLES

https://doi.org/10.1038/s41564-019-0372-2

Proteomic profiling of HIV-1 infection of human CD4+ T cells identifies PSGL-1 as an HIV restriction factor

Ying Liu[1,10], Yajing Fu[2,3,10], Qian Wang[4], Mushan Li[5], Zheng Zhou[3], Deemah Dabbagh[3], Chunyan Fu[1], Hang Zhang[1], Shuo Li[1], Tengjiang Zhang[1], Jing Gong[1], Xiaohui Kong[1], Weiwei Zhai[6,7], Jiaming Su[8], Jianping Sun[9], Yonghong Zhang[9], Xiao-Fang Yu[8], Zhen Shao[5], Feng Zhou[4*], Yuntao Wu[3*] and Xu Tan[1*]

Human immunodeficiency virus (HIV) actively modulates the protein stability of host cells to optimize viral replication. To systematically examine this modulation in HIV infection, we used isobaric tag-based mass spectrometry to quantify changes in the abundance of over 14,000 proteins during HIV-1 infection of human primary CD4+ T cells. We identified P-selectin glycoprotein ligand 1 (PSGL-1) as an HIV-1 restriction factor downregulated by HIV-1 Vpu, which binds to PSGL-1 and induces its ubiquitination and degradation through the ubiquitin ligase $SCF^{\beta\text{-}TrCP2}$. PSGL-1 is induced by interferon-γ in activated CD4+ T cells to inhibit HIV-1 reverse transcription and potently block viral infectivity by incorporating in progeny virions. This infectivity block is antagonized by Vpu via PSGL-1 degradation. We further show that PSGL-1 knockdown can significantly abolish the anti-HIV activity of interferon-γ in primary CD4+ T cells. Our study identifies an HIV restriction factor and a key mediator of interferon-γ's anti-HIV activity.

Human immunodeficiency virus (HIV) can successfully infect human CD4+ T cells and macrophages despite the highly evolved antiviral innate immunity in cells. A major component of host anti-HIV innate immunity are restriction factors, which are host proteins that block specific steps in the viral replication cycle[1–5]. Besides their HIV-blocking ability, these restriction factors often share three characteristics[6]. First, they are usually inducible by interferons (IFNs), the master signalling proteins of antiviral immunity. Second, genes encoding these factors have rapidly evolved because of the high selection pressure exerted by lentiviruses, which is reflected in the positive selection signatures in their amino acid sequences[7]. Third, HIV often possesses effective mechanisms to counteract these factors to survive in the host cells. Several HIV restriction factors have been identified so far, including tripartite motif-containing protein 5-α (TRIM5-α)[8], APOBEC3 (ref. [9]), tetherin[10], SAM domain and HD domain-containing protein 1 (SAMHD1)[11,12] and serine incorporator 3 (SERINC3)/SERINC5 (refs. [13,14]). Remarkably, HIV uses a similar strategy to remove at least three of these factors, APOBEC3, tetherin and SAMHD1. Specifically, HIV uses Vif, Vpu and Vpx to recruit Cullin-5 (CUL5)-, CUL1- and CUL4-based Cullin-RING E3 ligases (CRLs) to target APOBEC3, tetherin and SAMHD1 for degradation respectively[11,12,15–17].

Given the importance of the degradation of host restriction factors to the virus, we systematically profiled protein abundance in human primary CD4+ T cells during HIV-1 infection to discover new restriction factors. Mass spectrometry-based proteomic profiling of HIV-1 infection has been performed in cell lines[18,19] and on a limited scale in primary T cells[20,21], which have revealed several host factors involved in viral infection. Here, we applied a sensitive isobaric tag-based quantitative mass spectrometry technology[22] to perform proteomic profiling of human primary CD4+ T cells following HIV-1 infection. We quantitated over 14,000 proteins and uncovered a large cohort of novel candidate host factors involved in HIV-1 infection of primary T cells as well as previously known restriction factors, such as APOBEC3 family and tetherin. We conducted corresponding RNA sequencing (RNA-seq) analysis in comparison and found evidence of widespread alterations of host proteins by HIV-1 via post-transcriptional mechanisms. Our results provide a comprehensive view of the proteomic landscape changes during HIV-1 infection and generated many links of host proteins to HIV-1 infection. Among these host proteins, we focused on P-selectin glycoprotein ligand 1 (PSGL-1; also named SELPLG), a protein downregulated by HIV. We present evidence demonstrating that PSGL-1 is an HIV restriction factor that is specifically induced

[1]MOE Key Laboratory of Bioorganic Phosphorus Chemistry & Chemical Biology, Beijing Advanced Innovation Center for Structural Biology, School of Pharmaceutical Sciences, Tsinghua-Peking Center for Life Sciences, Center for Infectious Disease Research, School of Medicine, Tsinghua University, Beijing, China. [2]Key Laboratory of AIDS Immunology of National Health and Family Planning Commission, Department of Laboratory Medicine, The First Affiliated Hospital, China Medical University, Shenyang, China. [3]School of System Biology, George Mason University, Manassas, VA, USA. [4]Liver Cancer Institute, Zhongshan Hospital, Key Laboratory of Carcinogenesis and Cancer Invasion, Ministry of Education and Institutes of Biomedical Sciences, Fudan University, Shanghai, China. [5]Key Laboratory of Computational Biology, CAS-MPG Partner Institute for Computational Biology, Shanghai Institutes for Biological Sciences, Chinese Academy of Sciences, Shanghai, China. [6]Key Laboratory of Zoological Systematics and Evolution, Institute of Zoology, Chinese Academy of Sciences, Beijing, China. [7]Center for Excellence in Animal Evolution and Genetics, Chinese Academy of Sciences, Kunming, China. [8]Cancer Institute (Key Laboratory of Cancer Prevention and Intervention, China National Ministry of Education), Second Affiliated Hospital, School of Medicine, Zhejiang University, Hangzhou, Zhejiang, China. [9]Beijing You'an Hospital, Capital Medical University, Beijing, China. [10]These authors contributed equally: Ying Liu, Yajing Fu. *e-mail: zhou_feng@fudan.edu.cn; ywu8@gmu.edu; xutan@tsinghua.edu.cn

by IFN-γ and antagonized by HIV-1 Vpu via the E3 ligase SCF (Skp1, CUL1, F-box)$^{\beta\text{-TrCP2}}$.

Results

Proteomic profiling of CD4$^+$ T cells in HIV-1 infection. We recently developed a sensitive mass spectrometry platform that allows genome-scale proteomic profiling using fewer than 10^6 cells and thus enables the study of primary tissues and rare cell populations[22]. We used VSV-G-pseudotyped HIV-1 (NL4-3) with an enhanced green fluorescent protein (eGFP) reporter (VSV-G-HIV-GFP hereinafter) to infect about 10^8 activated human primary CD4$^+$ T cells and sorted the CD4$^+$ T cells by GFP using flow cytometry 48 h later. GFP$^+$ (G$^+$) cells and GFP$^-$ (G$^-$) cells, together with mock-infected and sorted cells (V$^-$), were immediately lysed and digested with trypsin before being labelled with iTRAQ reagents, mixed and subjected to mass spectrometry analyses (Fig. 1a). We performed four mass spectrometry runs (two replicate runs, two donors) and identified 14,455 proteins from at least one donor and 7,779 from both donors (Fig. 1b and Supplementary Data Set 1). To quantitate the changes in protein abundance between V$^-$, G$^-$ and G$^+$ cell populations, we used a statistical analysis method based on the mass spectrum peptide peak intensities and fold changes between cell populations (Supplementary Table 1 and Supplementary Data Set 2). Gene Ontology analysis of the proteins with changes in abundance among the three populations revealed the enrichment of proteins involved in IFN-α responses, IFN-γ responses, HIV-induced T cell apoptosis, G2/M checkpoint and antiviral responses (Supplementary Fig. 1a and Supplementary Data Set 3). Several HIV-1 proteins (Gag, Pol, Vif and Rev), as expected, are more abundant in G$^+$ cells than in G$^-$ cells (G$^+$ > G$^-$) (Fig. 1c) or in V$^-$ cells (G$^+$ > V$^-$) (Fig. 1d). We did not detect Vpu, Vpr and Tat, probably because they are short in amino acid sequences and, therefore, difficult to detect in mass spectrometry. Nef was also not detected, probably due to the high hydrophilicity of the trypsin-generated peptides of Nef. In addition, we found that CD4, known to be depleted by HIV-1 Vpu and Nef[23], and restriction factors known to be degraded by HIV-1, APOBEC3 family (A3G, A3F and A3C) and tetherin, were significantly downregulated in G$^+$ cells (Fig. 1c). By contrast, the level of SAMHD1, was not changed between G$^+$ cells and G$^-$ cells, as it is degraded by HIV-2 Vpx but not by HIV-1 (Fig. 1c). Conversely, we detected multiple IFN-stimulated genes (ISGs) upregulated in G$^-$ cells compared to V$^-$ cells (G$^-$ > V$^-$), including *MX1*, *MX2*, *OAS1*, *OAS2*, *OAS3* and *ISG15*, indicating IFN responses in G$^-$ cells (Fig. 1e and Supplementary Data Set 4). These ISG levels were lower in the G$^+$ cells than in the G$^-$ cells (G$^-$ > G$^+$), correlating with increased infection in G$^+$ cells. Another group of genes showing higher expression in G$^-$ cells than in V$^-$ cells are the fatty acid and cholesterol synthesis genes, including *FDFT1* (encoding squalene synthase), *HMGCS1* (encoding hydroxymethylglutaryl-CoA synthase) and *FASN* (encoding fatty acid synthase) (Fig. 1e), consistent with a previous report[24].

To further validate the results, we repeated the viral infections and flow cytometry sorting in both primary and Jurkat T cells, and used western blotting to confirm 12 hits identified from the proteomic profiling (Fig. 1f and Supplementary Fig. 1b). The hits were selected mainly based on their top *P* values and novelty. The western blotting results, with p24 as a control, demonstrated a pattern highly correlative with the mass spectrometry results. For example, the levels of KIF11 and hyaluronan-mediated motility receptor (HMMR), two proteins involved in cell motility, were confirmed to be elevated in G$^+$ cells (Fig. 1d,f and Supplementary Fig. 1b). The level of FDFT1, the squalene synthase regulating cholesterol biosynthesis, was also elevated in both G$^-$ cells and G$^+$ cells compared with V$^-$ cells (Fig. 1d–f and Supplementary Fig. 1b). In comparison, two subunits of PP2A phosphatase, PPP2R5A and PPP2R5D, were markedly decreased in G$^+$ cells, consistent with a recent report[19] (Fig. 1c,d,f and Supplementary Fig. 1b). The levels of four membrane proteins, PSGL-1, sialophorin (SPN; also known as leukosialin), CD3D and CD3E, and a transcription factor, TCF7, were also markedly decreased in G$^+$ cells compared to G$^-$ cells (Fig. 1c,f and Supplementary Fig. 1b). Nucleolar and spindle-associated protein 1 (NuSAP1) and cofilin, two intracellular proteins, show reduced abundance in both G$^-$ cells and G$^+$ cells compared to V$^-$ cells (Fig. 1c,f and Supplementary Fig. 1b). Interestingly, most of these validated protein level changes cannot be attributed to mRNA levels, suggesting post-transcriptional regulations (Supplementary Fig. 1c,d). Together, these results support the reliability of our proteomic profiling.

To assess the general correlation between protein levels and mRNA levels, we further performed RNA-seq analyses of primary CD4$^+$ T cells from three additional donors. Cells were infected and sorted as in the proteomic profiling. RNA-seq analyses yielded 16,129 genes, 75.8% of which (12,223) had also been identified in our proteomic profiling (Fig. 2a and Supplementary Data Set 5), demonstrating a significant overlap of genes/proteins discovered by the two profilings. In addition, genes with low RNA levels were also detected in our proteomic profiling, reflecting the sensitivity and depth of our proteomics methodology (Fig. 2b). The overall correlation of RNA abundance and protein abundance is high (Fig. 2c). However, there are sizeable differences between the two lists of differentially expressed genes at RNA and protein levels (Fig. 2d and Supplementary Data Sets 2 and 6). Although the two lists overlap significantly, the majority of the genes with differential RNA or protein levels do not share the two lists, suggesting widespread post-transcriptional regulations, which is consistent with our validations (Fig. 1f and Supplementary Fig. 1b–d).

Given that most antiviral proteins are ISGs, we analysed the overlaps of our proteomic hits with annotated ISGs[25] and found a significant overlap between the G$^-$ > V$^-$ group and ISGs (Fig. 2e and Supplementary Data Set 4). The overlap between the G$^+$ < G$^-$ group and the ISGs is also significant (Fig. 2e). In comparison, both the G$^+$ < G$^-$ and the G$^-$ > V$^-$ groups do not have significant overlaps with the IFN downregulated gene list (Fig. 2e and Supplementary Data Set 4). These analyses show that our proteomic hits enriched for ISGs.

Another characteristic of HIV-1 restriction factors is the positive selection signature of their gene sequences during evolution[26]. We compared our hits with a list of genes positively selected in the mammalian genomes[27] (Supplementary Data Set 7). We found a significant overlap of both the G$^-$ > V$^-$ and the G$^+$ < G$^-$ groups with positively selected genes (Fig. 2f). Remarkably, among the 21 genes overlapped between the G$^+$ < G$^-$ group and positively selected genes, at least 10 are known to be functionally associated with HIV-1 infection (*APOBEC3C*, *CD3E*[26], *CD3G*[26], *CD4*, *HLA-A*[28], *HLA-B*[28], *IFIT1* (ref. [29]), *RNASEL*[30], *SLAMF6*/*NTB-A*[31] and *SPN*[26]). All 10 genes have anti-HIV functions except *CD4*, which encodes the receptor for HIV and is downregulated by HIV Nef and Vpu (Supplementary Data Set 7). These results suggest that our proteomic results have identified genes with characteristics of antiviral factors.

Vpu promotes PSGL-1 ubiquitination and degradation. We were encouraged by the high recovery rate of genes functionally relevant to HIV-1 from the 21 genes overlapped between G$^+$ < G$^-$ group and positively selected genes[27], so we focused on one with a very high likelihood of positive selection (Supplementary Data Set 7), PSGL-1, for further analysis because: (1) PSGL-1 is specifically expressed in lymphocytes and myeloid cells, which are targets of HIV infection; (2) a previous profiling has found that PSGL-1 is downregulated in the membrane fraction of the HIV-1-infected CEM-T4 cell line[18]; and (3) PSGL-1 associates with HIV-1 Gag at the HIV-1 assembly sites[32]. The total protein level of PSGL-1 was downregulated by the replication-competent HIV-IIIB in MAGI cells overexpressing

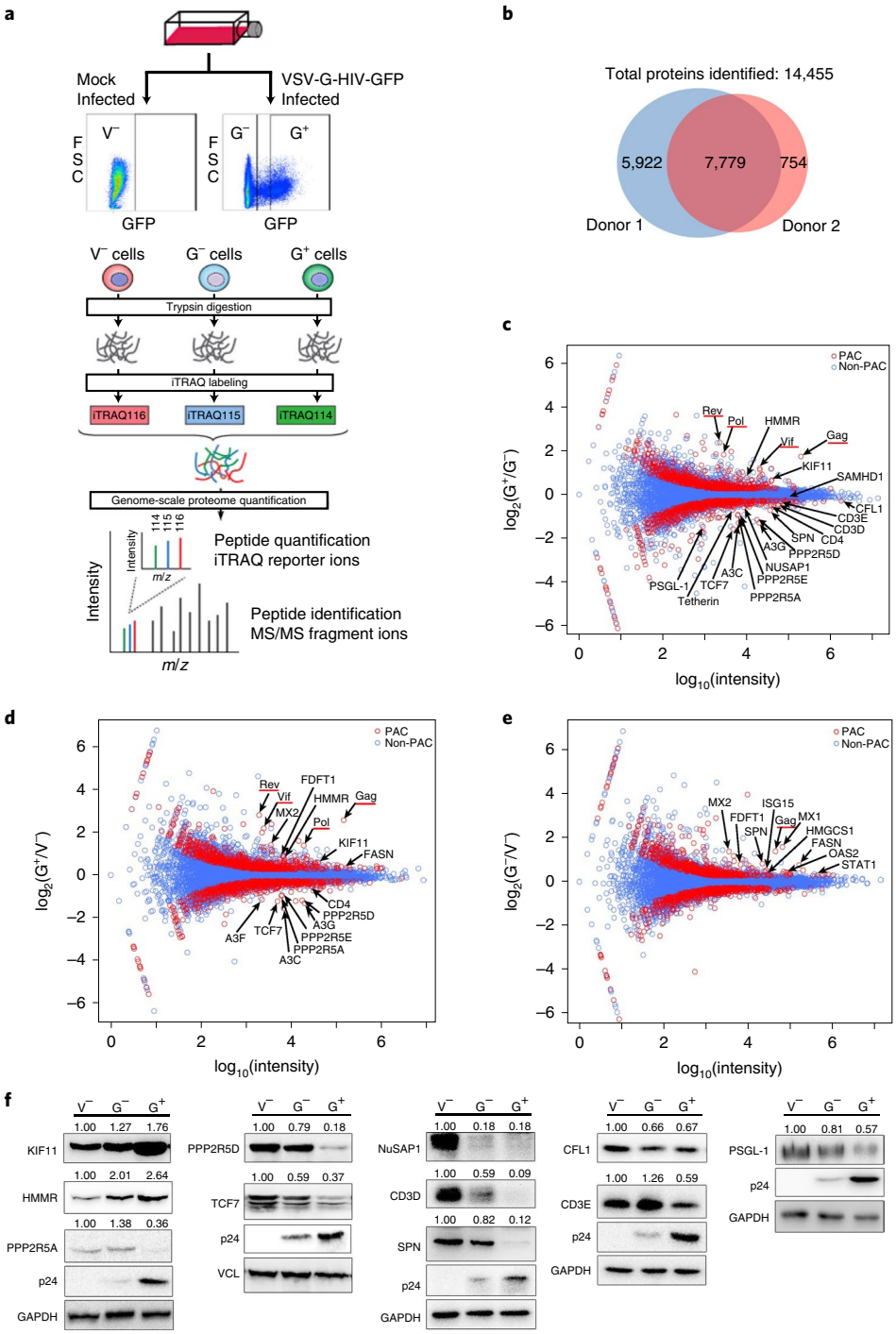

Fig. 1 | Proteomic profiling of HIV-1 infection in human primary CD4⁺ T cells. a, Experimental scheme of the proteomic profiling. FSC, forward scattering; MS/MS, tandem mass spectrometry; *m/z*, mass to charge ratio. **b**, Venn diagram of the identified proteins from two donors. **c**, Comparison for the protein profiling results of G⁻ and G⁺ cell populations. The colour of each dot represents a *P* value calculated based on the $\log_2$ ratio of the abundance of each protein in the two populations ($\log_2(G^+/G^-)$) (see Methods for the statistical test used). The best *P* values of all of the technical replicates are shown. The intensity is the normalized mean mass spectrometry peak intensity of each protein associated with the best *P* value among the four replicates. The viral proteins identified are underlined in red. CFL1, cofilin 1; non-PAC, proteins with no significant abundance changes; PAC, proteins with significant abundance changes. **d**, Same as **c**, except the comparison is between the G⁺ and V⁻ cell populations. **e**, Same as **c**, except the comparison is between the G⁻ and V⁻ cell populations. STAT1, signal transducer and activator of transcription 1. **f**, Validation of protein abundance changes in primary CD4⁺ T cells from three different donors. Vinculin (VCL) and GAPDH were used as loading controls. The numbers are the relative quantities of the intensities of the protein bands normalized to those of the loading controls. The quantities of the bands of the V⁻ cell samples were then normalized as 1.00. Data are representative of three different donors.

PSGL-1 without corresponding changes in the mRNA level (Fig. 3a and Supplementary Fig. 2a). Fluorescence-activated cell sorting (FACS) analysis of Jurkat cells that were infected by VSV-G-HIV-GFP also show a dose-dependent decrease in the level of PSGL-1 (Supplementary Fig. 2b). We then sought to identify which HIV protein caused PSGL-1 downregulation. Overexpression of Vpu,

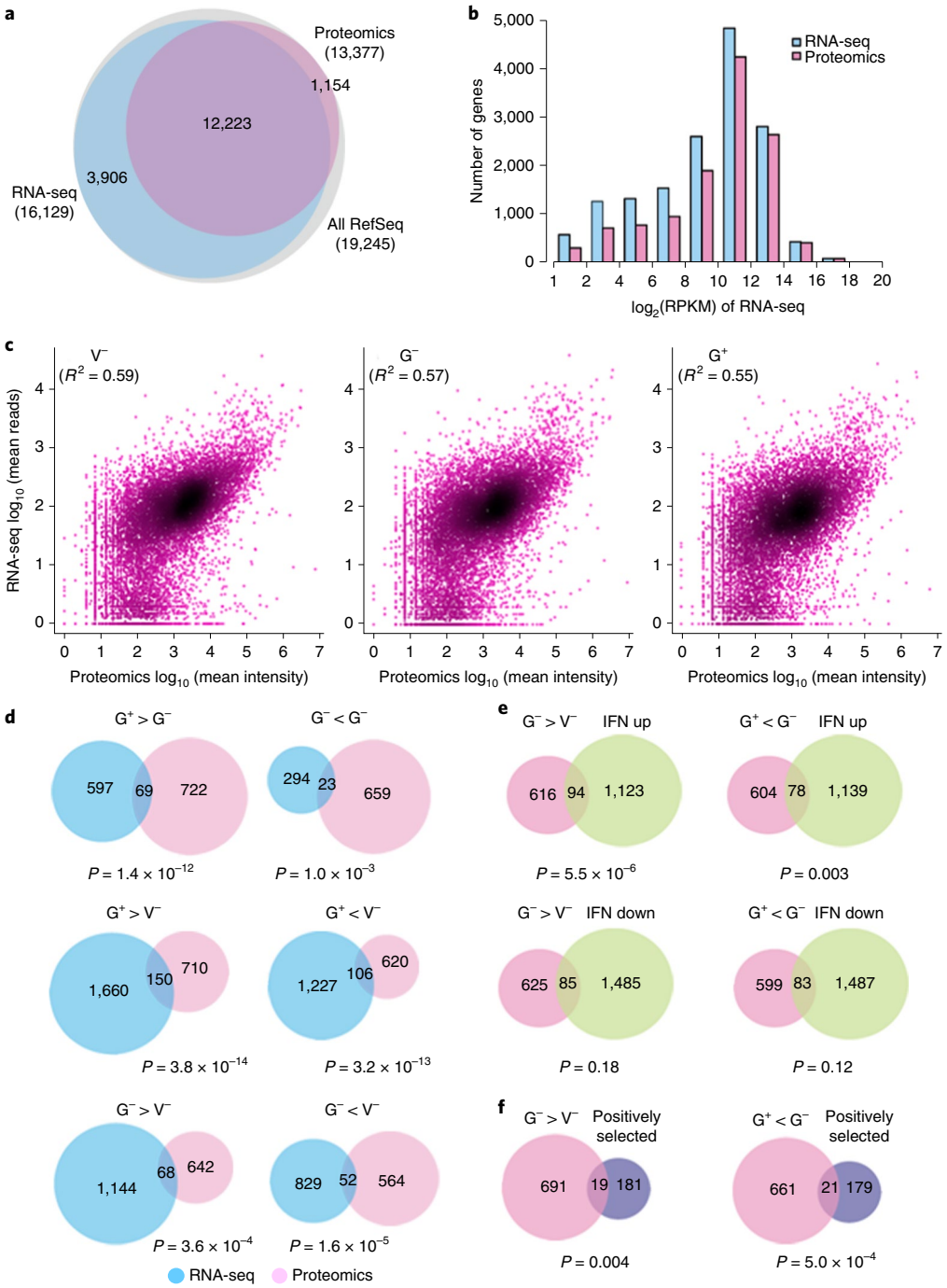

Fig. 2 | Comparison of proteomic profiling results with other large data sets for cross-validation and identification of candidate genes. a, Venn diagram showing the overlap of proteins identified in proteomic profiling and genes identified in RNA-seq (only those proteins and genes with records in the RefSeq database were counted). All RefSeq data indicate the total number of gene records in the RefSeq database. **b**, Distribution of genes or proteins based on the RNA-seq data reads count ($\log_2$(RPKM)). **c**, Linear regression correlation of the intensities of RNA-seq and proteomic profiling of each gene or protein of the three cell populations: V^-, G^- and G^+ ($n = 2$ for proteomic data and $n = 3$ for RNA-seq data). **d**, Venn diagrams of genes or proteins with differential RNA or protein abundance in the V^-, G^- and G^+ cell populations. **e**, Venn diagrams showing overlapping of proteins with differential protein abundance in the V^-, G^- and G^+ cell populations and proteins that are upregulated (up) or downregulated (down) by IFNs. **f**, Venn diagrams showing overlapping of proteins with differential protein abundance in the V^-, G^- and G^+ cell populations and genes that are positively selected in the mammalian genomes. The *P* values in **d**–**f** show the significance of the overlaps calculated with the hypergeometric test.

but not Nef, Vif, Vpr nor p55 Gag, significantly decreased PSGL-1 level in 293T cells (Fig. 3b and Supplementary Fig. 2c) and Jurkat cells (Supplementary Fig. 2d). These results were validated in primary $CD4^+$ T cells from two donors, in which HIV-1 infection can significantly decrease the endogenous PSGL-1 level (Fig. 3c and Supplementary Fig. 2e). By contrast, Vpu-deleted HIV (NL4-3 delVpu) had no effect on PSGL-1, suggesting a Vpu-dependent downregulation (Fig. 3c and Supplementary Fig. 2e). This Vpu dependence of PSGL-1 downregulation is also shown with flow cytometry analysis of VSV-G-HIV-GFP infection of primary $CD4^+$

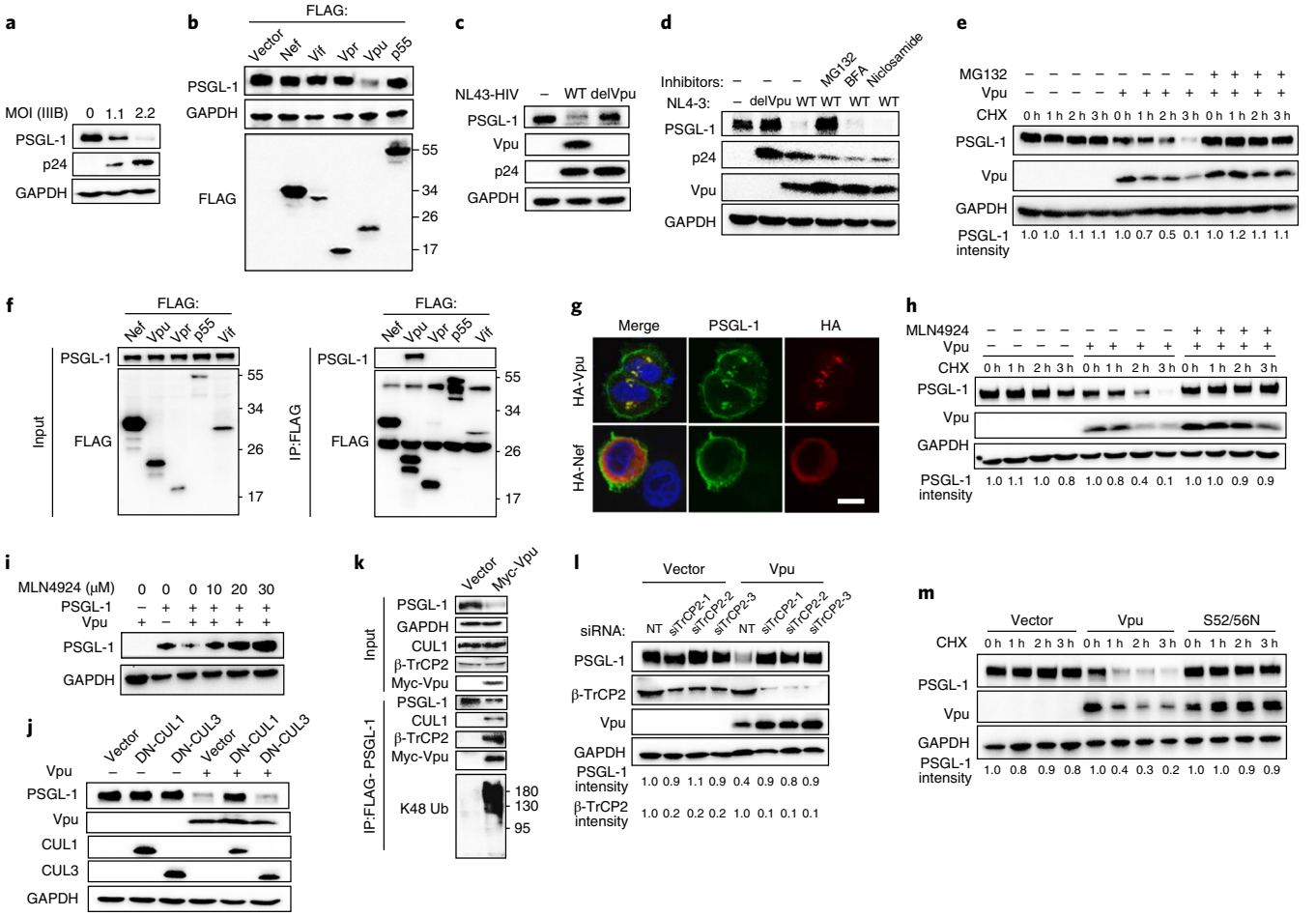

Fig. 3 | PSGL-1 is degraded by HIV-1 via ubiquitination by the Vpu-hijacked SCF$^{\beta\text{-TrCP2}}$ E3 ligase. a, Western blots of lysates of MAGI cells overexpressing a haemagglutinin (HA)-tagged PSGL-1 protein and infected by an increasing multiplicity of infection (MOI) of HIV-1 IIIB (0, 1.1 and 2.2). **b**, Western blots of lysates of 293T cells co-transfected with plasmids expressing PSGL-1 and one of the following HIV-1 proteins: Nef, Vif, Vpr, Vpu, p55-Gag or an empty vector. **c**, Western blots of lysates of primary CD4$^+$ T cells that were infected with NL4-3 (WT) or NL4-3 delVpu (delVpu) or mock-infected (–) for 48 h. **d**, Jurkat cells were infected with HIV-1 NL4-3 or NL4-3 delVpu or mock infected (—) for 48 h. MG132, bafilomycin (BFA) or niclosamide were added 6 h before the cells were harvested and analysed by western blotting. WT, wild type. **e**, 293T cells were co-transfected with plasmids expressing PSGL-1 and Vpu. A total of 18 h after the transfection, the cells were first treated with MG132 for 6 h and then with CHX for the indicated time before being harvested, and the cell lysates were analysed by western blotting. Empty vector (—) was used as a negative control for the Vpu-expressing vector (+). **f**, 293T cells were separately transfected with plasmids expressing PSGL-1 or a plasmid expressing FLAG-tagged Nef, Vif, Vpr, Vpu or p55-Gag. Two days after transfection, the two batches of cell lysates were mixed as indicated and HIV-1 proteins were immunoprecipitated (IP) with M2 anti-FLAG beads. **g**, 293T cells were co-transfected with plasmids expressing PSGL-1 and Vpu. Sixteen hours after transfection, cells were fixed, permeabilized and stained for PSGL-1 (PSGL-1 antibody) and Vpu (HA antibody) to observe the colocalization. Scale bar, 5 μm. **h**, 293T cells were treated with MLN4924 and then co-transfected with PSGL-1 and Vpu or an empty vector. One day after the transfection, the cells were treated with CHX and collected at the indicated time points. The cell lysates were analysed by western blotting. **i**, 293T cells were treated with MLN4924 at the indicated concentrations 24 h before the cells were transfected with plasmids expressing PSGL-1 and Vpu. Two days after transfection, the cells were harvested and analysed by western blotting. Empty vector (–) was used as a negative control for the Vpu- or PSGL-1-expressing vectors. **j**, Western blots of lysates of 293T cells transfected with plasmids expressing PSGL-1 and either DN-CUL1 or DN-CUL3 or an empty vector. The Vpu-expressing plasmid (+) or an empty vector (—) is also transfected as indicated. **k**, 293T cells were transfected with plasmids expressing FLAG-PSGL-1 and Myc-Vpu or an empty vector. Two days after transfection, cells were treated with MG132 for 8 h and then the lysates were immunoprecipitated with M2 anti-FLAG beads. The cell lysates and precipitated proteins were analysed by western blotting. **l**, 293T cells were transfected with three siRNAs targeting β-TrCP2 or a non-targeting siRNA (NT). One day post-transfection, cells were then transfected with plasmids expressing PSGL-1 and Myc-Vpu or an empty vector. Two days post-plasmid transfection, cells were harvested and analysed by western blotting. **m**, 293T cells were co-transfected with plasmids expressing PSGL-1 and Vpu, or the Vpu S52/56N mutant or an empty vector. One day after transfection, cells were treated with CHX and collected at the indicated time points. The results of **a**–**m** are representative of at least three independent experiments. Values of molecular mass indicated in **b**,**f**,**k** are in kDa.

T cells (Supplementary Fig. 2f). In addition, in Jurkat cells, NL4-3-induced PSGL-1 degradation can be rescued by the proteasome inhibitor MG132, but not by lysosome inhibitors (Fig. 3d), suggesting proteasomal degradation. Furthermore, a cycloheximide (CHX) chase experiment confirmed that PSGL-1 is indeed destabilized by Vpu (Fig. 3e). We further found that PSGL-1 co-immunoprecipitated specifically with Vpu (Fig. 3f) and also colocalized with Vpu in intracellular compartments (Fig. 3g). Given that Vpu is known to hijack the SCF$^{\beta\text{-TrCP1}/\beta\text{-TrCP2}}$ E3 ligase[33,34], we tested whether PSGL-1 degradation might be dependent on this E3 ligase. Indeed, a

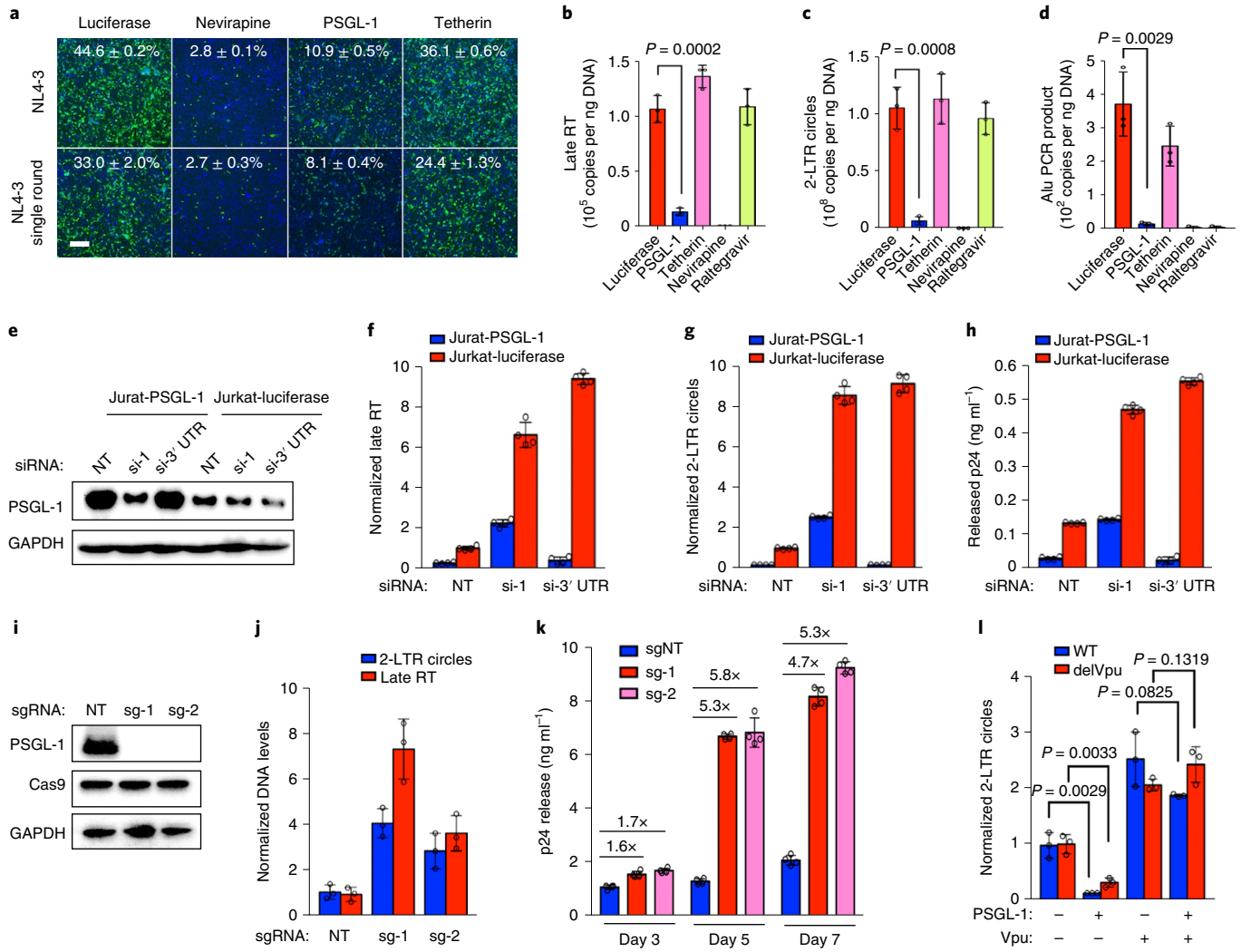

Fig. 4 | PSGL-1 in target cells inhibits HIV-1 replication, starting from DNA synthesis. a, MAGI cells in 12-well plates were transfected with 300 ng per well of luciferase-, PSGL-1- and tetherin-expressing plasmids. Two days after transfection, the cells were infected with HIV-1 NL4-3 or NL4-3-ΔEnv-eGFP pseudotyped with HIV-1 Env for 48 h before being stained for p24 (green)/nuclei (blue) and imaged. A reverse transcription inhibitor, nevirapine, was used as a control. The numbers indicate mean infection rates ± standard deviations. Scale bar, 50 μm. $n = 4$. **b**–**d**, MAGI cells transfected with plasmids expressing luciferase, PSGL-1 or tetherin as in **a** were infected with HIV-1 NL4-3 for 12 h or 24 h before the DNA was extracted to measure late reverse transcription (RT) products (**b**) and 2-LTR circles (**c**), respectively, or for 72 h before the DNA was extracted to measure HIV-1 DNA integration by Alu PCR (**d**). Nevirapine and raltegravir were used as controls. $n = 3$. **e**, Jurkat cells stably expressing PSGL-1 or luciferase were electroporated with one of two siRNAs targeting PSGL-1 (si-1 and si-3′ UTR) or a non-targeting siRNA (NT). The PSGL-1 protein levels were determined using western blot. The results are representative of three independent experiments. **f**,**g**, qRT–PCR quantification of the late reverse transcription products (**f**) and 2-LTR circles (**g**) of Jurkat-luciferase and Jurkat-PSGL-1 cells electroporated with different siRNAs and cultured for 48 h and then infected with HIV-1 IIIB for 24 h. $n = 4$. **h**, ELISA quantification of released p24 from Jurkat-luciferase and Jurkat-PSGL-1 cells electroporated with different siRNAs and cultured for 48 h and then infected with HIV-1 IIIB for 72 h. $n = 4$. **i**, Western blot to validate the PSGL-1 protein level of two PSGL-1 knockout Jurkat cell lines. sg-1 and sg-2 are two sgRNAs targeting PSGL-1. The results are representative of three independent experiments. **j**, qRT–PCR quantification of late reverse transcription products or 2-LTR circles in PSGL-1 knockout or control Jurkat cells infected with HIV-1 NL4-3 for 24 h. $n = 3$. **k**, ELISA quantification of released p24 from PSGL-1 knockout or control Jurkat cells infected with HIV-1 NL4-3 at 3, 5 or 7 d post-infection. The numbers above the bars indicate the fold of change bewteen the two values indicated by the bars. **l**, qRT–PCR quantification of 2-LTR circles of MAGI cells stably expressing luciferase or PSGL-1 and transfected with Vpu or empty vector for 48 h and then infected with NL4-3 and NL4-3 delVpu. $n = 3$. For all bar graphs, the mean ± standard deviation is shown.

pan-CRL inhibitor, MLN4924, rescued PSGL-1 from Vpu-induced degradation (Fig. 3h,i). In addition, overexpressing a dominant negative CUL1 amino-terminal domain (DN-CUL1)[35], which inhibits all SCF ligases, also rescued PSGL-1 from degradation. As a control, dominant negative CUL3 (DN-CUL3)[35] did not affect the PSGL-1 level (Fig. 3j). Vpu overexpression induced PSGL-1 ubiquitination (Fig. 3k and Supplementary Fig. 2g), correlating with a Vpu-dependent co-immunoprecipitation of PSGL-1 with CUL1 and β-TrCP2 (Fig. 3k). Moreover, the Vpu-induced PSGL-1 ubiquitination and degradation can be reversed by short interfering RNA (siRNA)-mediated knockdown of β-TrCP2 (Fig. 3l and Supplementary Fig. 2g). By contrast, knockdown of β-TrCP1 has no effect (Supplementary Fig. 2h). A Vpu mutant (S52N/S56N or S52/56N) defective for β-TrCP1/2 binding[34] lost the ability to promote PSGL-1 ubiquitination (Supplementary Fig. 2i,j) and degradation (Fig. 3m and Supplementary Fig. 2k), similar to the effect of this mutation on tetherin degradation (Supplementary Fig. 2l). However, the binding between Vpu and PSGL-1 is different from

Vpu–tetherin binding, as evidenced by the Vpu A14L mutant, which can abolish tetherin binding[36] but not PSGL-1 binding and degradation (Supplementary Fig. 2k–m).

PSGL-1 inhibits HIV-1 reverse transcription. The Vpu-induced degradation of PSGL-1 suggests a function in HIV-1 infection or transmission. Indeed, transient expression of PSGL-1 in the target cells reduced the infection rate of HIV-NL4-3 and HIV-IIIB (Fig. 4a and Supplementary Fig. 3a). This inhibition is not affected by Vpu as NL4-3 and NL4-3 delVpu were similarly inhibited, suggesting that the inhibition occurs before Vpu expression. As a control, transient expression of tetherin caused a significant inhibition of NL4-3 delVpu, but not wild-type virus nor a single-round NL4-3 virus. To examine which step of the HIV-1 life cycle is inhibited by PSGL-1, we first tested cellular entry of HIV-1 using a β-lactamase (BlaM)-based entry assay[37] and found no significant decrease in HIV-1 entry due to PSGL-1 overexpression in both Jurkat and TZM-bl target cells (Supplementary Fig. 3b,c). This is consistent with that PSGL-1 also inhibited a VSV-G-pseudotyped NL4-3 virus (Supplementary Fig. 3a). By contrast, HIV-1 reverse transcription was significantly decreased by PSGL-1 overexpression (Fig. 4b and Supplementary Fig. 3d–f). The steps following reverse transcription, the nuclear accumulation and chromosomal integration of HIV-1 DNA, were also significantly reduced (Fig. 4c,d and Supplementary Fig. 3g,h). These inhibitions were similar for both NL4-3 and NL4-3 delVpu, consistent with the late expression of Vpu. As a consequence of PSGL-1's inhibition of the early events of HIV-1 infections, HIV-1 gene expression was also significantly reduced, as measured by immunofluorescence staining of p24 in one-round infection of MAGI cells (Fig. 4a and Supplementary Fig. 3a). We further performed loss-of-function tests of the role of PSGL-1 in HIV-1 replication. Electroporation of PSGL-1 siRNAs markedly increased the levels of HIV-1 late reverse transcription, two copies of the long terminal repeat (2-LTR) circles and released p24 in Jurkat cells (Fig. 4e–h, red bars). These enhancements were due to an on-target effect of RNA interference, as overexpressing the open reading frame of PSGL-1 without the 3′ untranslated region (UTR) could rescue the effect of an siRNA targeting the 3′ UTR of PSGL-1 (si-3′ UTR), but not that of an siRNA targeting the coding region (si-1) (Fig. 4e–h, blue bars). We also generated CRISPR (clustered regularly interspaced short palindromic repeats)–Cas9 (CRISPR-associated protein 9)-mediated PSGL-1 knockout of Jurkat cells using two single-guide RNAs (sgRNAs) (Fig. 4i). Compared to a cell line expressing control sgRNA, these PSGL-1 knockout cell lines show higher susceptibility to HIV-1 infection (Fig. 4j,k). To further support the anti-HIV activity of PSGL-1, we performed immunofluorescence co-staining of PSGL-1 and HIV-1 p24 and observed a clear separation of PSGL-1 staining from p24 staining in infected MAGI cells stably expressing exogenous PSGL-1 (Supplementary Fig. 3i). Together, these data strongly support the restrictive nature of PSGL-1 on HIV-1 replication, probably starting at reverse transcription.

PSGL-1 potently inhibits the infectivity of progeny HIV-1 virions. We found that exogenous expression of Vpu can abolish the inhibition of HIV-1 DNA synthesis by PSGL-1 (Fig. 4l), consistent with Vpu-mediated PSGL-1 degradation. However, in real infection, this inhibition by PSGL-1 would precede Vpu expression as Vpu is not present in the incoming virions. We suspect that there is a late-acting inhibition of HIV-1 by PSGL-1 that is antagonized by Vpu. Indeed, we observed that virions produced from PSGL-1-expressing 293T cells were dramatically less infectious than those from control cells expressing tetherin, as measured by their infections of TZM-bl reporter cells, even the virions were normalized by p24 levels (Fig. 5a). Consistent with Vpu-mediated PSGL-1 degradation, NL4-3 delVpu virions had an even greater loss of infectivity than wild-type NL4-3 (Fig. 5a). We further observed a stronger infectivity inhibition by PSGL-1 using the Rev-A3R5-GFP T cell line (Fig. 5b,c), a Rev-dependent HIV-1 reporter cell line[38] (Supplementary Fig. 4a). Again, NL4-3 delVpu was more sensitive to the inhibition than wild-type NL4-3 (Fig. 5b,c). Consistently, PSGL-1 knockout in producer Jurkat cells significantly boosted the infectivity of NL4-3 virus and even more significantly that of NL4-3 delVpu virus, supporting that, in Jurkat cells, the infectivity of NL4-3 delVpu virus is suppressed more strongly by PSGL-1 (Fig. 5d). This infectivity inhibition suggests that the progeny virions may be negatively imprinted by PSGL-1 from the producer cells, which is consistent with PSGL-1 being transferred from the producer cells to the target cells by the virus (Fig. 5e). To confirm the association of PSGL-1 with progeny virions, we used density gradient centrifugation to purify the virions released from 293T cells and observed the co-sedimentation of PSGL-1 with purified virions (Supplementary Fig. 4b). We further used an ascorbate peroxidase 2 (APEX2)-based labelling method to observe APEX2-tagged PSGL-1 in the virions under electron microscopy[39]. We first confirmed that APEX2-tagged PSGL-1 and the control APEX2-tagged tetherin retained their activities to inhibit HIV-1 and that APEX2-tagged PSGL-1 is transferred to the infected cells by the virions (Supplementary Fig. 4c). The electron microscopy images of the HIV-1 virions revealed that PSGL-1 is located to the periphery of the virions (Fig. 5f), with NL4-3 delVpu virions demonstrating more PSGL-1 than wild-type virions (Fig. 5g). As a control, no tetherin was visibly associated with the new virions as expected. Together, these data support that PSGL-1 is incorporated into progeny virions and inhibits viral infectivity. This inhibition is partially relieved by Vpu via PSGL-1 degradation.

Fig. 5 | PSGL-1 in producer cells inhibits the infectivity of HIV-1 progeny virions. a, 293T cells in 12-well plates were co-transfected with 1 μg per well of pNL4-3 or pNL4-3 delVpu proviral plasmids and plasmids expressing PSGL-1 or tetherin at the indicated dosages. Two days after transfection, the supernatants were collected and normalized for the p24 amount to infect TZM-bl cells for 48 h before the infection units were measured with the β-galactosidase assay. $n = 3$. Data shown as the mean ± standard deviation. **b**,**c**, 293T cells in 12-well plates were co-transfected with 1 μg per well of pNL4-3 or pNL4-3 delVpu proviral plasmids and plasmids expressing PSGL-1 at the indicated dosages. Two days after transfection, the supernatants were collected and normalized for the p24 amount to infect Rev-A3R5-GFP cells for 72 h before the infection rate was measured by FACS. The FACS plots are shown in **b** and the normalized infection rates are shown in **c**. PI, propidium iodide. The results shown are representative of three independent experiments. **d**, PSGL-1 knockout or control Jurkat cells were infected with the NL4-3 or NL4-3 delVpu virus. The supernatants were collected 72 h post-infection and normalized for the p24 amount to infect TZM-bl cells for 48 h before the infection units were measured with the luciferase assay. $n = 3$. Data shown as the mean ± standard deviation. **e**, 293T cells in 12-well plates were co-transfected with 1 μg per well of pNL4-3 or pNL4-3 delVpu proviral plasmids and 100 ng per well of plasmids expressing PSGL-1 or tetherin or an empty vector. Two days after transfection, the supernatants were collected and normalized for p24 to infect MAGI cells for 48 h. The samples from the transfected 293T cells and the lysates of the infected MAGI cells were analysed by western blotting. Data shown are representative of three independent experiments. **f**, Electron microscopy images of 293T cells transfected with the plasmids expressing the indicated viral genomes and genes. Two representative images are shown for each group. The white arrows indicate PSGL-1-positive viral particles. Scale bar, 0.5 μm. **g**, Quantification of the percentage of PSGL-1-positive viral particles in electron microscopy images from PSGL-1 + pNL4-3 and PSGL-1 + pNL4-3 delVpu groups from panel **f**. $n = 10$. Data shown as the mean ± standard deviation.

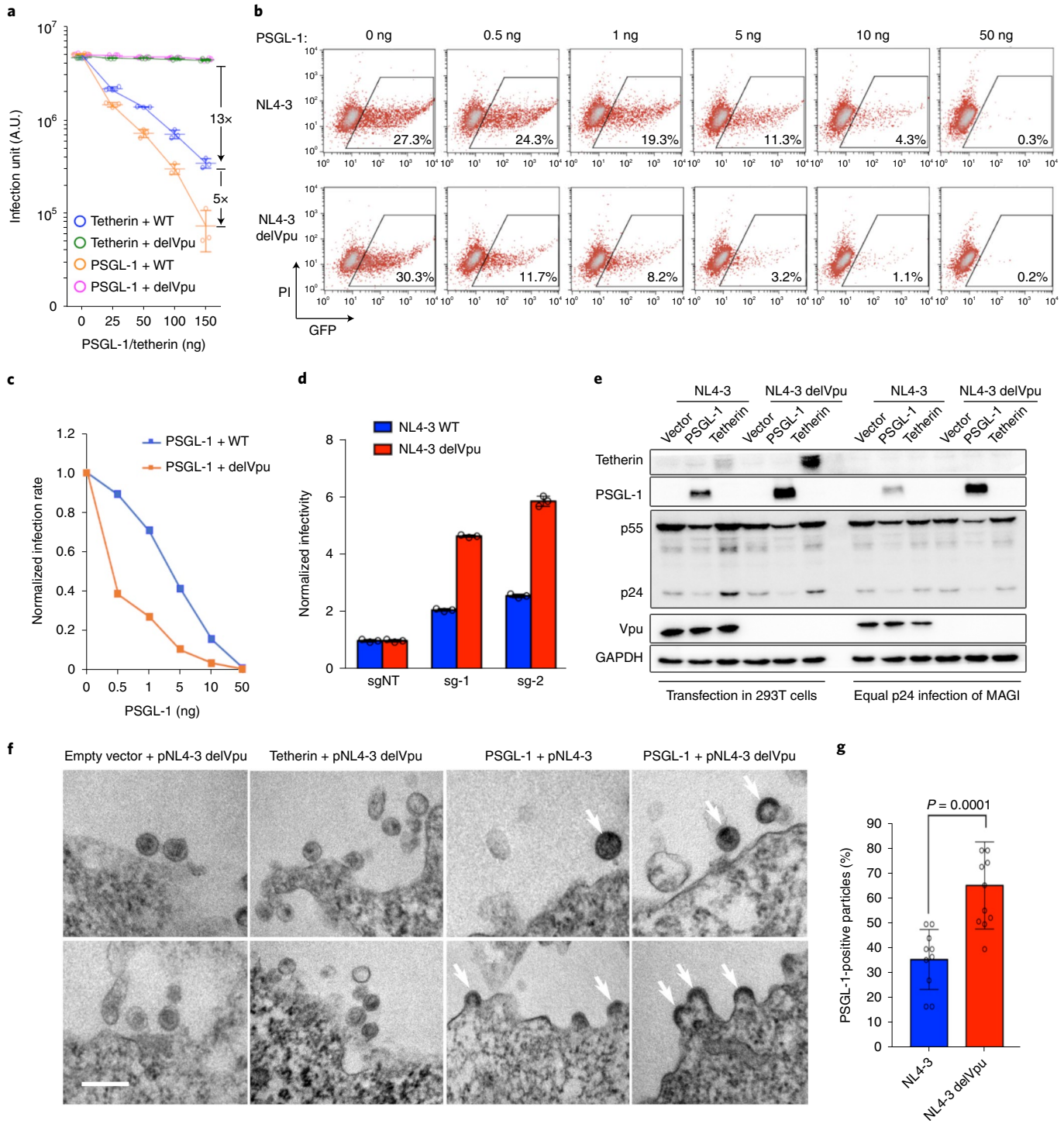

PSGL-1 is induced by IFN-γ and mediates the anti-HIV activity of IFN-γ. The expression level of PSGL-1 is high in T cell lines and primary T cells, but low in 293T cells and HeLa-based cell lines (Fig. 6a and Supplementary Fig. 5a). In addition, PSGL-1 mRNA and protein levels were significantly reduced when T cells were activated (Fig. 6a,b and Supplementary Fig. 5a–c), which correlates with an increased susceptibility to HIV-1 infection of activated T cells. As previously identified restriction factors are induced by IFNs, we tested whether this is true for PSGL-1. Interestingly, in both Jurkat cells and resting CD4$^+$ T cells, *PSGL1* mRNA levels are not induced by IFNs (Supplementary Fig. 5d,e). However, in activated CD4$^+$ T cells, PSGL-1 is strongly induced by IFN-γ (Fig. 6c and Supplementary Fig. 5f). By contrast, IFN-α does not seem to induce PSGL-1 expression in activated CD4$^+$ T cells (Supplementary Fig. 5g). It is worth noting that the PSGL-1 levels in the overexpression experiments (Fig. 4a–d) are comparable to the level induced by IFN-γ and, therefore, are physiologically relevant (Supplementary Fig. 5h). We tested the role of PSGL-1 in the anti-HIV activities of IFN-γ in activated primary CD4$^+$ T cells by electroporation of siRNAs. First, PSGL-1 knockdown significantly promoted HIV-1 infection in untreated primary CD4$^+$ T cells from two donors as measured by late reverse transcription and p24 release (Fig. 6d–f and Supplementary Fig. 5i,j), confirming the results in cell lines. Importantly, PSGL-1 knockdown also abolished the inhibition of HIV-1 DNA synthesis by IFN-γ (Fig. 6e) and significantly blunted the

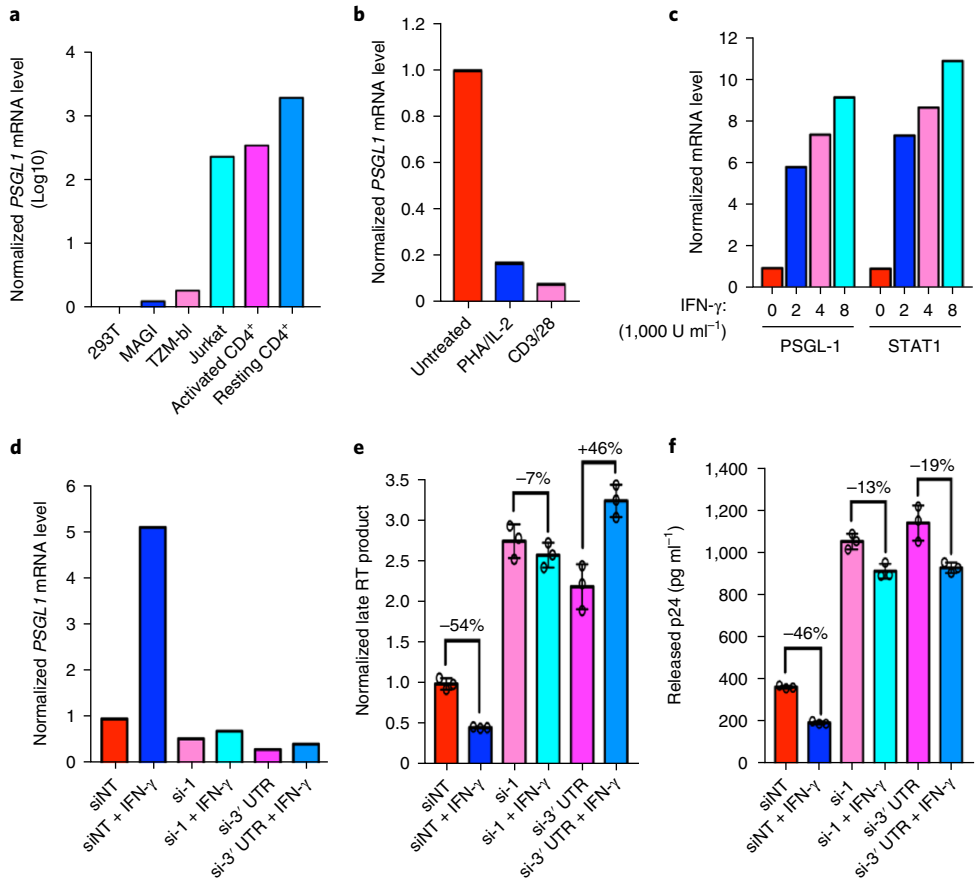

Fig. 6 | PSGL-1 mediates the anti-HIV activity of IFN-γ in activated primary CD4⁺ T cells. a, qRT–PCR quantification of *PSGL1* mRNA levels in cell lines and primary CD4⁺ T cells, resting or activated, with PHA/IL-2 or CD3/CD28 antibodies. The mRNA level was normalized to that of GAPDH. **b**, qRT–PCR quantification of *PSGL1* mRNA levels in primary CD4⁺ T cells, resting or activated, with PHA/IL-2 or CD3/CD28 antibodies. **c**, qRT–PCR quantification of *PSGL1* and *STAT1* mRNA levels of activated T cells treated with recombinant IFN-γ for 12 h. The mRNA levels were first normalized to that of GAPDH and then normalized to the level of the untreated sample (IFN-γ = 0 U ml^{-1}). **d**–**f**, Activated primary CD4⁺ T cells were treated or untreated with IFN-γ for 12 h before being electroporated with two different siRNAs targeting PSGL-1 or non-targeting control siRNA (siNT) for 48 h. The cells were then either extracted for the qRT–PCR quantification of *PSGL1* mRNA (**d**), infected with HIV-1 NL4-3 for 24 h before the DNA was extracted to measure late reverse transcription products (**e**) or for 72 h before the supernatant was collected to measure p24 release by ELISA (**f**). $n = 3$. Data are representative of at least three independent experiments. Data shown as the mean ± standard deviation (**e**,**f**).

inhibition of p24 release by IFN-γ (Fig. 6f and Supplementary Fig. 5i). These data support that PSGL-1 is a key component of the antiviral mechanisms of IFN-γ.

Discussion

Our sensitive isobaric tag-based mass spectrometry method enabled a comprehensive and deep proteomic profiling of the proteome of human CD4⁺ T cells during HIV-1 infection. The recovery of multiple known HIV-1 restriction factors, host factors and ISGs supports the robustness and utility of our method. Furthermore, a direct comparison with RNA-seq profiling has proven the comprehensiveness and depth of our proteomic profiling. Remarkably, the majority of the protein changes are not reflected in the mRNA levels, suggesting widespread post-transcriptional manipulations of host proteins by HIV-1 and validates the value of proteomic profiling. This observation is consistent with HIV-1 hijacking the ubiquitin ligases to ubiquitinate and degrade restriction factors. The same mechanism may also explain upregulation of host proteins, as endogenous substrates of the virus-hijacked E3 ligases would be competed off from the E3 ligases. We analysed known endogenous substrates of CUL5–RBX1 E3 ligases[40], which are hijacked by HIV-1 Vif to target APOBEC3 proteins. The majority (77%) of the endogenous substrates are upregulated during HIV-1 infection, probably due to the displacement of the endogenous substrates by Vif from the E3 ligase (Supplementary Fig. 6). The rationale for HIV-1 to repeatedly hijack the ubiquitin–proteasome system might be the high efficiency of the ubiquitination and degradation of restriction factors, which are critical for HIV-1 to evade the innate intracellular defences[41].

We established PSGL-1 as an HIV-1 restriction factor that is ubiquitinated by HIV-1 Vpu via the E3 ligase SCF$^{\beta\text{-TrCP2}}$. We demonstrate that PSGL-1 is induced by IFN-γ in activated CD4⁺ T cells and inhibits HIV-1 DNA synthesis and virion infectivity. The infectivity inhibition is more potent: a low level of PSGL-1 overexpression can lead to a significant reduction of virion infectivity. Vpu is made during the late stages of the HIV-1 life cycle to partially neutralize the restriction by PSGL-1. We further identified PSGL-1 as a specific IFN-γ-induced antiviral restriction factor. IFN-γ has been primarily considered as an immunomodulatory cytokine, and its role in innate immune defence against HIV-1 has only started to be mechanically dissected[42,43]. Future studies should unveil the molecular mechanism of PSGL-1's antiviral activities and the conservation and sequence requirement of the counter-PSGL-1 activity of Vpu among HIV and simian immunodeficiency virus strains. Further understanding of the interaction between Vpu and PSGL-1 may present potential targets for developing new anti-HIV drugs.

Methods

Cells and cell culture. For cell culture, 293T cells (from the American Type Culture Collection), TZM-bl and MAGI cells (from the NIH AIDS Reagents Repository) were cultured in DMEM supplemented with 10% heat-inactivated FBS, 6 mM L-glutamine, and penicillin and streptavidin. Jurkat E6.1 cells were cultured in RPMI-1640 containing 10% FBS, 6 mM L-glutamine, and penicillin and streptavidin. Rev-A3R5-GFP indicator cells (a gift from Virongy) were cultured in RPMI with 1 mg ml^{-1} geneticin (G418) and 1 μg ml^{-1} puromycin. Peripheral blood mononuclear cells were isolated from healthy human donors using Ficoll-Paque PLUS (GE Healthcare). CD4$^+$ T cells were purified from peripheral blood mononuclear cells using anti-human CD4 magnetic beads (Miltenyi) and then cultured in RPMI supplemented with 10% heat-inactivated FBS, β-mercaptoethanol and 6 mM L-glutamine. Naive CD4$^+$ T cells were activated with CD3/CD8 beads (Invitrogen) and human recombinant interluekin-2 (IL-2; 30 U ml^{-1}; Roche) for 72 h or by phytohaemagglutinin A (PHA; 4 μg ml^{-1}; Sigma) and IL-2 (20 U ml^{-1}; Roche) for 72 h.

Sample preparation for proteomic analysis. Human primary CD4$^+$ T cells were stimulated with anti-CD3/CD28 beads (Invitrogen) and human recombinant IL-2 (30 U ml^{-1}; Roche) for 7–10 d. About 100 million cells were infected with VSV-G-HIV-GFP virus at a multiplicity of infection of 5 with spinoculation at 2,000*g* for 2 h. For the mock infection group, about 10 million cells were mock-infected with media. Two days after the infection, the cells were sorted for GFP intensity and the sorted cells were collected. From these cells, the proteins were extracted with 8 M urea in 0.1 M NH_4HCO_3. The proteins were reduced by dithiothreitol at 10 mM for 60 min in the dark and then alkylated by methyl methanethiosulfonate (Thermo Fisher Scientific) at 20 mM for 30 min. The protein was incubated with trypsin at 37 °C overnight for digestion. The peptides were loaded onto Oasis HLB reverse phase plates (Waters) to remove urea and other salts. The resulting peptides were labelled with 4-plex iTRAQ reagents (AB Sciex). In this study, G$^+$, G$^-$ and V$^-$ cells were labelled with iTRAQ reagents 114, 115 and 116, respectively. After labelling, all peptides were mixed together and loaded into an online three-dimensional chromatography platform for in-depth proteomic quantification.

Multi-dimensional separation and data acquisition. The nanoscale three-dimensional online chromatography platform was modified to small scale for these experiments. It consists of a first-dimension reversed-phase column (capillary with a 150-μm internal diameter packed with 10 cm of 5-μm diameter of XBridge (Waters) C18 resin), a second-dimension strong anion exchange column (150-μm internal diameter, 10 cm of 10-μm diameter POROS10HQ (AB Sciex) resin) and a third-dimension reversed-phase column (25-μm internal diameter, 120 cm of 5-μm diameter monitor C18 (Column Engineering), integrated 1-μm diameter emitter tip). The final dimension ran at 1–3 nl min^{-1} with a 600-min gradient from 3% buffer B to 50% buffer B (buffer A = 0.1% formic acid; buffer B = acetonitrile with 0.1% formic acid). The downstream TripleTOF 5600$^+$ (AB Sciex) was set in information-dependent mode for data acquisition. The top 50 precursors (charge state of +2 to +5, >100 counts) in each mass spectrometry scan (800 ms, scan range: 350–1,500 m/z) were subjected to mass spectrometry/mass spectrometry (minimum time 140 ms, scan range: 100–1,400 m/z). The electrospray voltage was 2.4 kV.

Data processing and protein identification. The mass spectrometry data were subjected to search against the SwissProt database (downloaded on 23 June 2016) with ProteinPilot V.4.5 (AB Sciex). Official HGNC gene symbols were also included in the database. The search parameter was set to 'iTRAQ 4-plex (peptides labelling) with 5,600 TripleTOF'. The peptide spectra match false discovery rate was used to filter the peptides identified for further analysis. Only those peptides with scores at or above a peptide spectra match false discovery rate threshold of 0.01 were kept for data analysis. In this study, we also removed peptides that can be assigned to more than one gene. After that, we summed the intensity of each iTRAQ reporter ion for the peptides that can only be assigned to a single gene to generate a ratio for each gene.

Protein quantification. In this study, we utilized the previously developed 'error model'[44] with modification to determine the significance for the difference in protein expression level. Briefly, we first built an 'error model' from an independent mass spectrometry data set generated from the mouse lymphoid cell line BAF3 to measure the technical and systematic error of protein quantification. The same amount of whole-cell lysate of the samples was labelled across all iTRAQ channels, and their iTRAQ-reported ion intensities were measured by mass spectrometry. The obtained data were used to plot the $\log_2$ ratios of protein intensities for all detected proteins against their mean $\log_2$ intensities between two proteomic profiles. These systematic errors should follow a zero-centred normal distribution $N(0, \sigma^2)$. The variance σ^2 can be estimated as

$$\sigma^2 = \Psi(\theta, U) = \exp(\theta_1 + \theta_2 \cdot U)$$

$\sigma^2 = \Psi(\theta, U_i)$ is computed from the global variance function for protein i, as an estimation of the contribution of technical and systematic errors in its $\log_2$ ratio. θ represents the function used to fit the variance of the noise extracted from the 1/1 experiment. U_i represents the average intensity of protein i under two conditions. A two-tailed P value is calculated for each protein to represent the significance of its intensity change, as the probability of observing an equal or greater value than the absolute value of its R_i from normal distribution $N(0, \sigma_i^2 = \Psi(\theta, U_i))$ using the formula

$$P = \int_{|R_i|}^{+\infty} \frac{1}{\sqrt{2\sigma_i \pi}} * e^{-x^2/(2\sigma_i^2)} dx$$

R_i represents the $\log_2$ ratio for the intensity of protein i under two conditions. This model was validated with comparison with a ribosome profiling data set also generated from mouse embryonic stem cells (Liu et al., unpublished data). We then applied this model to the ratio of each protein measured in the following experiments for statistical assessment. For the data that we obtained for T cells and HIV-infected T cells, we used the median iTRAQ reporter ion ratio from these data as a normalization factor for data analysis. The proteomics experiments were conducted as two biological replicates and two technical replicates for each biological replicate. A technical replicate is a duplication of the mass spectrometry run of the same sample to control for the variance in the mass spectrometry analysis. A protein was included in the list of proteins with abundance changes if the iTRAQ $\log_2$ ratio was either higher than 0.26 or lower than −0.26, that the total iTRAQ intensity was over 300 counts and that the P value derived in 'error model' from each donor was lower than 0.05 in at least two runs from all four runs. Adjustment of the P value by Benjamini–Hochberg correction for multiple testing is also provided in Supplementary Data Set 2. The different coverages between the samples of the two donors are due to the different cell numbers or infection rate of the two donors' samples, in addition to person-to-person variation in protein expression; thus, we did not restrict our analysis to proteins that were differentially expressed in both donors. It is important to note that, because the intensity ratios measured by iTRAQ-based mass spectrometry can be distorted during precursor ion isolation, variation in some protein expression may be underestimated in the data. The fold change associated to the most significant P value of each protein is included in the Supplementary Tables and the dot plots in Fig. 1. The P value adjusted with the Benjamini–Hochberg method was also calculated and provided in the Supplementary Tables.

RNA-seq analysis. Total RNA from cells (from three donors) that were infected and sorted into V$^-$, G$^-$ and G$^+$ cell populations as described above was isolated using RNeasy Plus Mini Kit (Qiagen) following the manufacturer's protocol. The RNA-seq library was prepared using the Truseq v2 LT Sample Prep Kit (Illumina). The sequencing was performed at the Beijing Genomics Institute (Shenzhen, China) using RNA-seq technology as follows: (1) 200 ng total RNA per sample were used to enrich poly(A) mRNA using oligo (dT) magnetic beads. (2) The purified mRNA was fragmented and reverse transcribed into double-strand cDNA using N6 random primer. (3) The double-strand cDNA was treated by a traditional process, including end repairing with phosphate at the 5′ end and an extra 'A' at the 3′ end, and ligation with an adaptor with an extra 'T' at the 3′ end. (4) Two specific primers were used to amplify the ligation product. (5) The double-stranded PCR products were heat denatured to single strands and circularized by splint oligo and DNA ligase. (6) Sequencing was performed on the prepared library, and the nine libraries were sequenced on the Illumina HiSeq 4000 platform based on sequencing by synthesis with 100-bp paired-end reads. The sequencing reads from all RNA-seq experiments were aligned to the human (hg18) reference genome by TopHat. Differential gene expression analyses were performed using DEseq or Cufflinks using fold change ≥ 1.5 and $P \leq 0.01$ as the cut-off.

Plasmids, transfection and viral particle production. The plasmids used in this study are listed in the table below. For exogenous expression in mammalian cells, human PSGL-1 or its truncated form, or luciferase or tetherin were cloned into a pLenti-CMV vector with an N-terminal haemagglutinin tag and FLAG tag, or a PLX-304 vector with a carboxy-terminal V5 tag. The vectors were transfected into cell lines using Neofect transfection reagent following the manufacturer's protocol (Neofect Biotech). For the transfection of plasmids into Jurkat cells, 0.3 million Jurkat cells were seeded into 1 ml RPMI-1640 and mixed with a mixture containing 3 μl of a formulation of lipid nanoparticles recently developed[45], 1.4 μl lipid nanoparticles and 2 μl siRNA (20 μmol l^{-1}) or 500 ng plasmids. The HIV genes *nef*, *vif*, *vpu*, *vpr* and *p55* were cloned from pNL4-3 and inserted into a pLenti-CMV vector. Full-length Vpu was also expressed using a pcDNA3.0 vector with an N-Myc tag, and its point mutations (S52/56N and A14L) were introduced by site-directed mutagenesis followed by digestion of parental DNA with DpnI. DN-CUL1 and DN-CUL3 were cloned into pcDNA3.0. VSV-G-NL4-3 viral particles were produced by transfection of 293T cells in a T75 flask with 20 μg pNL4-3-ΔEnv-eGFP, 5 μg pCG-VSV-G and 25 μl DNA Neofect transfection reagent. NL4-3 one-round viral particles were produced by transfection of 293T cells in a T75 flask with 20 μg pNL4-3-ΔEnv-eGFP and 5 μg PNL-ΔΨ-Env (gp160). NL4-3 and delVpu viral particles were produced by transfection of 293T cells in a T75 flask with 20 μg pNL4-3 or pNL4-3 delVpu. Short hairpin RNA (shRNA)-expressing, sgRNA-expressing and open reading frame-expressing plasmids were packaged into

lentiviral particles in each well of a six-well plate with 10 μg pLKO.1, lentiCRISPR v2, pLX304 or pCMV backbone vectors, 2 μg pCG-VSV-G, 1 μg pCMV-Tat, 1 μg pCMV-Rev and 1 μg pCMV-Gagpol. For packaging of Vpr-BlaM viral particles, 10 μg pNL4-3, 3.4 μg pMM310-Vpr-BlaM and 1.7 μg pAdvantage were transfected into each well of a six-well plate. Twenty-four hours after transfection, the medium was removed. Viral supernatants were collected after another 24 h and filtered at 0.45 μM. The HIV-IIIB virus was provided by N. Yan (University of Texas Southwestern Medical Center) and amplified in the H9 cell line.

shRNA and siRNA. All of the shRNAs were bought from Sigma, and all of the siRNAs were purchased from GenePharma. The shRNAs were cloned into the lentiviral vector pLKO.1, and sgRNAs were cloned into the plentiCRISPR-v2 vector. For siRNA transfection, Lipofectamine RNAiMax (Invitrogen) was used following the manufacturer's protocol, and the knockdown efficiency was qualified by qRT–PCR 72 h after transfection. For siRNA nucleofection, the siRNAs were transfected into Jurkat E6.1 cells or peripheral blood mononuclear cells using the Amaxa Nucleofector following the manufacturer's protocols (Lonza).

The shRNAs sequences used in this study are as below:
shNT: CGTGATCTTCACCGACAAGAT
shPSGL-1-1: AGAGGTCTGTTCATACCCTTT
shPSGL-1-2: AGCCAGCAATTTGTCCGTCAA
The sgRNA sequences used in this study:
sgNT (non-targeting control): TTTGAAGTATGCCTCAAGGT
sgPSGL-1-1: TGGGGGAGTAATTACGCACG
sgPSGL-1-2: ATCTAGGTACTCATATTCGG
The siRNA sequences used in this study are as below:
siNT sense: UUCUCCGAACGUGUCACGUTT
siNT antisense: ACGUGACACGUUCGGAGAATT
siPSGL-1-1 sense: GCCACUAUCUUCUUCGUGUTT
siPSGL-1-1 antisense: ACACGAAGAAGAUAGUGGCTT
siPSGL-1-3′ UTR sense: CAGGAGGCCAUUUACUUGATT
siPSGL-1-3′ UTR antisense: UCAAGUAAAUGGCCUCCUGTT
siβ-TrCP1-1 sense: GCACUUGCGUUUCAAUAAUTT
siβ-TrCP1-1 antisense: AUUAUUGAAACGCAAGUGCTT
siβ-TrCP1-2 sense: GGCACAUAAACUCGUAUCUTT
siβ-TrCP1-2 antisense: AGAUACGAGUUUAUGUGCCTT
siβ-TrCP1-3 sense: CCAUUAAAGUUGCGGUAUUTT
siβ-TrCP1-3 antisense: AAUACCGCAACUUUAAUGGTT
siβ-TrCP2-1 sense: CCCAAAGAUUAUCCAGGAUTT
siβ-TrCP2-1 antisense: AUCCUGGAUAAUCUUUGGGTT
siβ-TrCP2-2 sense: GGAUGUGAACACGGGUGAATT
siβ-TrCP2-2 antisense: UUCACCCGUGUUCACAUCCTT
siβ-TrCP2-3 sense: GCCAAACACCUACCCAGAATT
siβ-TRCP2-3 antisense: UUCUGGGUAGGUGUUUGGCTT.

Antibodies and beads. The following antibodies were used for cell cytometry, immunostaining or western blotting: anti-PSGL-1 (1:200; sc-13535, Santa Cruz), anti-Eg5 (1:1,000; ab171963, Abcam), anti-HMMR (1:1,000; ab124729, Abcam), anti-PPP2R5A (1:1,000; ab72028, Abcam), anti-PPP2R5D (1:1,000; ab88075, Abcam), anti-FDFT1 (1:1,000; ab195046, Abcam), anti-TCF7 (1:500; 2203, Cell Signaling), anti-vinculin (1:3,000; V4505, Sigma), anti-SPN (1:200; PA526628, Thermo Fisher Scientific), anti-CD3D (1:500; ab109531, Abcam), anti-CD3E (1:500; ab52959, Abcam), anti-NuSAP1 (1:500; A302-595A, Bethyl), anti-cofilin (1:500; 5175, Cell Signaling), anti-APOBEC3G (1:500; 11231, NIH AIDS Reagent Program), anti-ubiquitin (1:300; ab140601, Abcam), anti-β-TrCP2 (1:1,000; ab154070, Abcam), anti-BTRC (1:1,000; sc-8863, Santa Cruz), anti-p24 (1:1,000; 1513, NIH AIDS Reagent Program), anti-Vpu (VPU-101AP, FabGennix), anti-actin (1:1,000; sc-8432, Santa Cruz), anti-GAPDH (1:1,000; TA-08, ZSGB-Bio), anti-V5 (1:1,000; CW0095A, CWBio), anti-Myc (1:1,000; AT0023-2, CMCTAG) and anti-FLAG (1:1,000; F1804, Sigma). For immunoprecipitation and the pull-down assay, protein A-agarose beads (sc-2001, Santa Cruz), anti-FLAG M2 magnetic beads (M8823, Sigma) and anti-Myc magnetic beads (B2630, Bimake) were used. The fluorescent secondary antibodies used in this study were Alexa Fluor 488 goat anti-rabbit IgG (H+L) (1:1,000; A-11008, Molecular Probes), Alexa Fluor 647 donkey anti-rabbit IgG (H+L) (1:1,000; A-31573, Molecular Probes), Alexa Fluor 488 goat anti-mouse IgG (H+L) (1:1,000; A-11001, Molecular Probes), Alexa Fluor 594 goat anti-mouse IgG (H+L) (1:1,000; A-11005, Molecular Probes) and Alexa Fluor 568 goat anti-rabbit IgG (H+L) (1:1,000; A-11010, Molecular Probes).

Immunoprecipitation assay. For the immunoprecipitation assay using anti-FLAG-tag antibody, cells in each well of six-well-plates were transfected with 2 μg pLX304-PSGL-1, pCMV-empty vector, pCMV-Nef, pCMV-Vif, pCMV-Vpr, pCMV-Vpu or pCMV-p55 individually. The cells were lysed with RIPA buffer (50 mM Tris-Cl, pH 7.4, 150 mM NaCl, 1% NP-40, 0.5% sodium deoxycholate, 0.1% SDS and protease inhibitor cocktail) 48 h after transfection. The PSGL-1-overexpressing 293T cell lysate was mixed with cell lysate of cells expressing one of the HIV proteins of pCMV-empty vector and incubated with 20–30 μl M2 anti-FLAG magnetic beads (M8823, Sigma) at 4 °C overnight. The beads were washed three times the next day and boiled in 1× SDS–PAGE buffer at 95 °C for 10 min. For the co-immunoprecipitation of β-TrCP1/β-TrCP2 with Myc-Vpu/Myc-Vpu S52/56N, cells in six-well plates were co-transfected with pCMV-β-TrCP1/pCMV-β-TrCP2 and the Myc-Vpu/Myc-Vpu S52/56N mutation. The cell lysates were incubated with M2 anti-FLAG beads and wash three times the next day. For the detection of PSGL-1 ubiquitination, cells in six-well plates were transfected with siRNAs (final concentration: 20 nM) for 48 h, then transfected with 2 μg pLX304-PSGL-1 and 1 μg pCMV-Vpu or pCMV-empty vector. MG132 was added to the plate 24 h after transfection and remained in the medium for the next 24 h. For the co-immunoprecipitation assay using anti-Myc magnetic beads (B26301, Bimake), cells were co-transfected with Myc-Vpu or the Myc-Vpu A14L mutation and pCMV-PSGL-1 and pCMV-tetherin. Forty-eight hours post-transfection, the cell lysates were incubated with 40 μl anti-Myc beads overnight and wash three times with RIPA buffer.

Flow cytometry. For the cells infected with NL4-3-VSV-G or A3R5 cells infected with the HIV-1 virus, cells are fixed in 2% paraformaldehyde in PBS for 20 min in the dark, and washed twice with PBS and then analysed on a Becton Dickinson LSR Fortessa flow cytometer (fluorescence channels: FITC). For the calculation of the PSGL-1 expression, cells were fixed and washed, then incubated with anti-PSGL-1 antibody (1:200; sc-13535, Santa Cruz) in 4 °C for 30 min and washed twice. Then, the cells were incubated with Alexa Fluor 594 goat anti-mouse IgG (H+L) (1:1,000; A-11005, Molecular Probes) at room temperature and in the dark for 20 min and washed twice and analysed by cell cytometry (fluorescence channels: phycoerythrin).

Inhibitor treatments of cells. For all of the inhibitor experiments, the inhibitor dosages were first tested by Cell TiterGlo (Promega) to determine a non-toxic dose range. For the proteasomal and lysosomal inhibitors treatment, MLN4924 (HY-70062, MCE) was added 2 h post-infection or plasmids transfection; MG132 (20 μM; HZB2119-5, Harveybio), BFA (200 nM; S7046, Selleck) and niclosamide (50 μM; S3030, Selleck) were added 6 h before cells were harvested. For the CHX chase experiment, CHX (10 μg ml^{-1}; C7698, Sigma) were added 24 h post-plasmid transfection. For the IFN-γ/α and activation, cells were exposed to different concentrations of IFN-γ/α (Peprotech) for 12 h for *PSGL1* mRNA quantification and for 24 h for PSGL-1 protein quantification. For the measurement of the HIV-1 life cycle, for positive controls, nevirapine (10 μg ml^{-1}; SML0097, Sigma) or raltegravir (10 μM; CDS023737, Sigma) or T20 (1 μg ml^{-1}; NIH AIDS Reagents Program) were added 2 h prior to the infection.

BlaM assay. Vpr-BlaM NL4-3 was produced as previously described[37]. For infection of Jurkat-E6.1 cells, 2×10^5 Jurkat cells in each well of 12-well plates were incubated with the NL4-3 virus for 2 h at 37 °C. The cells were washed twice with PBS and then 0.5 ml 1× CCF4-AM dye solution (K1095, Life Technologies) in phenol-free DMEM/HEPES/2% FBS was added to the cells. The cells were incubated at 11 °C overnight, then washed twice with PBS, fixed in 2% paraformaldehyde in PBS for 20 min in the dark and analysed on a Becton Dickinson LSR Fortessa flow cytometer (fluorescence channels: Pacific Blue and AmCyan).

Confocal microscopy. For HIV p24 immunofluorescence staining, 6×10^3 MAGI cells were seeded into each well of 96-well plates. Forty-eight hours after infection, the cells were fixed in 4% paraformaldehyde in PBS, permeated in 0.2% Triton X-100 and stained with p24 antibody (mAB-183 for the NIH AIDS Reagents Repository) overnight at 4 °C. The cells were washed twice with PBS and then stained with Alexa Fluor 488 goat anti-mouse IgG (H+L) at room temperature in the dark for 1 h. The cells were finally stained with DAPI (1 μg ml^{-1}) in the dark for 10 min and analysed on an ArrayScan VTI 700 (Thermo Scientific). For the Vpu–PSGL-1 colocalization experiment, cells were fixed 16 h post-infection and stained and imaged as described above.

Real-time PCR amplification. Quantitative real-time PCR analyses of the following genes were carried out with the SYBR qPCR enzyme (Q311-02, Vazyme) and data were analysed by the Bio-Rad CFX96 system. The primer sets were as follows:

PSGL1 forward primer: 5′-TCCTCCTGTTGCTGATCCTACTG-3′;
PSGL1 reverse primer: 5′-TACTCATATTCGGTGGCCTGTCT-3′;
STAT1 forward primer: 5′-CAGCTTGACTCAAAATTCCTGGA-3′;
STAT1 reverse primer: 5′-TGAAGATTACGCTTGCTTTTCCT-3′.
A3G forward primer: 5′-GCATCGTGACCAGGAGTATGA-3′;
A3G reverse primer: 5′-GTCAGGGTAACCTTCGGGT-3′;
HMMR forward primer: 5′-ATGATGGCTAAGCAAGAAGGC-3′;
HMMR reverse primer: 5′-TTTCCCTTGAGACTCTTCGAGA-3′;
TCF7 forward primer: 5′-AGAAACGAATCAAAACAGCTCCT-3′;
TCF7 reverse primer: 5′-CGGGATTTGTCTCGGAAACTT-3′;
SPN forward primer: 5′-CTGTCTTCGTTAGCTGCCTG-3′;
SPN reverse primer: 5′-GCTCCTGACCACAGCAAGATAC-3′;
KIF11 forward primer: 5′-TCCCTTGGCTGGTATAATTCCA-3′;
KIF11 reverse primer: 5′-GTTACGGGGATCATCAAACATCT-3′;

PPP2R5A forward primer: 5′-TGCTAACATCTTCCGTACACTTC-3′;
PPP2R5A reverse primer: 5′-CCTCAAGCGTGGGTTCATCC-3′;
PPP2R5D forward primer: 5′-ACTTCGTGTCAGACCCACTCA-3′;
PPP2R5D reverse primer: 5′-CTCAGGGTAAATGGCCTCAGT-3′;
CD25 forward primer: 5′-GTGGGGACTGCTCACGTTC-3′;
CD25 reverse primer: 5′-CCCGCTTTTTATTCTGCGGAA-3′;
CD38 forward primer: 5′-CAACTCTGTCTTGGCGTCAGT-3′;
CD38 reverse primer: 5′-CCCATACACTTTGGCAGTCTACA-3′.

For the quantification of early reverse transcription products, the following primers were used. The amplifications were carried out with the SYBR-Green qPCR enzyme (Q311-02, Vazyme) and data were analysed by the Bio-Rad CFX96 system. The sample preparations were performed following published protocol[46].

Early reverse transcription forward primer: 5′-GGCTAACTAGGGAACCCACTG-3′;
Early reverse transcription reverse primer: 5′-GCTAGAGATTTTCCACACTGACTAA-3′.

For the measurement of viral late reverse transcription products and 2-LTR circles, the following primers were used for a TaqMan qRT–PCR protocol[47]:

Late reverse transcription forward primer: 5′-TGTGTGCCCGTCTGTTGTGT-3′;
Late reverse transcription reverse primer: 5′-GAGTCCTGCGTCGAGAGAGC-3′;
Late reverse transcription probe: 5′-(FAM)-CAGTGGCGCCCGAACAGGGA-3′.
2-LTR forward primer: 5′-AACTAGGGAACCCACTGCTTAAG-3′;
2-LTR reverse primer: 5′-TCCACAGATCAAGGATATCTTGTC-3′;
2-LTR probe: 5′-(FAM)-ACACTACTTGAAGCACTCAAG-3′.
Mitochondrial forward primer: 5′-ACC-CACTCCCTCTTAGCCAATATT-3′;
Mitochondrial reverse primer: 5′-GTAGGGCTAGGCCCACCG-3′;
Mitochondrial probe: 5′-(TET)CTAGTCTTTGCCGCCTGCGAAGCA(TAMRA)-3′.

For the Alu qPCR, the first round of PCR was performed using:
Alu forward primer: 5′-GCCTCCCAAAGTGCTGGGATTACAG-3′ and
HIV *gag* reverse primer: 5′-GTTCCTGCTATGTCACTTCC-3′.
Then dilute the PCR products 100–200 folds to perform a second round of qPCR using:
LTR(R) forward primer: 5′-TTAAGCCTCAATAAAGCTTGCC-3′;
LTR (U5) reverse primer: 5′-GTTCGGGCGCCACTGCTAGA-3′ and
Alu probes: 5′-FAM-CCAGAGTCACACAACAGACGGGCACA-TAMRA-3′.

p24 ELISA. Cells (2×10^5) were seeded onto a 24-well plate and infected with HIV-IIIB, NL4-3 or NL4-3 delVpu for 6 h, then washed twice. The supernatant was collected for the measurement of p24 after 48 h or 72 h using a commercial p24 ELISA kit (Sinobiological). For the virus packaged by 293T cells in a 12-well plate, cells were transfected with 1 μg pNL4-3 or pNL4-3 delVpu proviral plasmids and different doses of plasmids expressing PSGL-1 or tetherin. Eight hours post-transfection, cells were washed twice and the medium was replaced. Forty-eight hours post-transfection, the supernatant was collected for p24 measurement.

HIV virion fractionation. 293T cells in 15 cm^2 were co-transfected with 10 μg pNL4-3 or pNL4-3 delVpu and 1 μg PSGL-1 expressing vector or an empty vector as control. Virion-particle-containing supernatants were harvested at 48 h post-co-transfection and filtered through a 0.45-μm filter. Filtered supernatants were concentrated by ultracentrifuged at 100,000*g* for 2 h and virion pellets were resuspended in PBS. Opti-prep gradients (D1556, Sigma) were prepared in 1.2% increments from 6% to 18%. Virions were placed onto the top of gradient fractions and centrifuged for 2 h at 250,000*g* in a SW41 Ti rotor (Beckman). Gradient fractions were collected from the top of the gradient (1 ml for 1 fraction) and then precipitated with tricholoroacetic acid (T4885, Sigma) and pre-chilling acetone, resuspended in 1× loading dye and analysed by western blotting.

Electron microscopy. The APEX2 expressing plasmid was provided by Peng Zou (Peking University). APEX2 constructs were transfected into 293T cells with the HIV proviral plasmids pNL4-3 or pNL4-3 delVpu. The electron microscopy sample preparation were following published protocol[48]. Briefly, cells were fixed with 2% (v/v) glutatraldehyde for 60 min and then incubated with 20 mM glycine for 5 min. After that, cells were kept in a fresh solution containing 1× DAB (0.5 mg ml^{-1}) and 10 mM H_2O_2 for 30 min. The following incubation time of OsO_4 was shortened to 10 min from the published protocol to avoid the APEX2 signals being affected by the OsO_4 signals. Images were obtained using a Hitachi transmission electron microscope at 80 kV.

Statistical analysis. All experiments have been repeated at least three times unless otherwise specified. All of the bar graphs are shown with the mean ± standard deviations. Unpaired, two-tailed *t*-test was used to calculate the *P* value unless otherwise specified. The significance (*P* value) of the overlaps between multiple gene sets was calculated based on the hypergeometric distribution by performing statistical software R with the function named 'phyper'.

Reporting Summary. Further information on research design is available in the Nature Research Reporting Summary linked to this article.

Code availability

The computational code used in this study is available from the corresponding authors upon request.

Data availability

The data that support the findings of this study are available from the corresponding authors upon request. The raw proteomic data have been uploaded to the ProteomeXchange data repository with the ID number: PXD011233.

Received: 25 June 2018; Accepted: 16 January 2019;
Published online: 04 March 2019

References

1. Malim, M. H. & Bieniasz, P. D. HIV restriction factors and mechanisms of evasion. *Cold Spring Harb. Perspect. Med.* **2**, a006940 (2012).
2. Yan, N. & Chen, Z. J. Intrinsic antiviral immunity. *Nat. Immunol.* **13**, 214–222 (2012).
3. Towers, G. J. & Noursadeghi, M. Interactions between HIV-1 and the cell-autonomous innate immune system. *Cell Host Microbe* **16**, 10–18 (2014).
4. Altfeld, M. & Gale, M. Jr. Innate immunity against HIV-1 infection. *Nat. Immunol.* **16**, 554–562 (2015).
5. Simon, V., Bloch, N. & Landau, N. R. Intrinsic host restrictions to HIV-1 and mechanisms of viral escape. *Nat. Immunol.* **16**, 546–553 (2015).
6. Harris, R. S., Hultquist, J. F. & Evans, D. T. The restriction factors of human immunodeficiency virus. *J. Biol. Chem.* **287**, 40875–40883 (2012).
7. Daugherty, M. D. & Malik, H. S. Rules of engagement: molecular insights from host–virus arms races. *Annu. Rev. Genet.* **46**, 677–700 (2012).
8. Stremlau, M. et al. The cytoplasmic body component TRIM5α restricts HIV-1 infection in Old World monkeys. *Nature* **427**, 848–853 (2004).
9. Sheehy, A. M., Gaddis, N. C., Choi, J. D. & Malim, M. H. Isolation of a human gene that inhibits HIV-1 infection and is suppressed by the viral Vif protein. *Nature* **418**, 646–650 (2002).
10. Neil, S. J., Zang, T. & Bieniasz, P. D. Tetherin inhibits retrovirus release and is antagonized by HIV-1 Vpu. *Nature* **451**, 425–430 (2008).
11. Hrecka, K. et al. Vpx relieves inhibition of HIV-1 infection of macrophages mediated by the SAMHD1 protein. *Nature* **474**, 658–661 (2011).
12. Laguette, N. et al. SAMHD1 is the dendritic- and myeloid-cell-specific HIV-1 restriction factor counteracted by Vpx. *Nature* **474**, 654–657 (2011).
13. Rosa, A. et al. HIV-1 Nef promotes infection by excluding SERINC5 from virion incorporation. *Nature* **526**, 212–217 (2015).
14. Usami, Y., Wu, Y. & Gottlinger, H. G. SERINC3 and SERINC5 restrict HIV-1 infectivity and are counteracted by Nef. *Nature* **526**, 218–223 (2015).
15. Yu, X. et al. Induction of APOBEC3G ubiquitination and degradation by an HIV-1 Vif–Cul5–SCF complex. *Science* **302**, 1056–1060 (2003).
16. Mitchell, R. S. et al. Vpu antagonizes BST-2-mediated restriction of HIV-1 release via β-TrCP and endo-lysosomal trafficking. *PLoS Pathog.* **5**, e1000450 (2009).
17. Van Damme, N. et al. The interferon-induced protein BST-2 restricts HIV-1 release and is downregulated from the cell surface by the viral Vpu protein. *Cell Host Microbe* **3**, 245–252 (2008).
18. Matheson, N. J. et al. Cell surface proteomic map of HIV infection reveals antagonism of amino acid metabolism by Vpu and Nef. *Cell Host Microbe* **18**, 409–423 (2015).
19. Greenwood, E. J. et al. Temporal proteomic analysis of HIV infection reveals remodelling of the host phosphoproteome by lentiviral Vif variants. *eLife* **5**, e18296 (2016).
20. Chan, E. Y. et al. Dynamic host energetics and cytoskeletal proteomes in human immunodeficiency virus type 1-infected human primary CD4 cells: analysis by multiplexed label-free mass spectrometry. *J. Virol.* **83**, 9283–9295 (2009).
21. Wojcechowskyj, J. A. et al. Quantitative phosphoproteomics reveals extensive cellular reprogramming during HIV-1 entry. *Cell Host Microbe* **13**, 613–623 (2013).
22. Zhou, F. et al. Genome-scale proteome quantification by DEEP SEQ mass spectrometry. *Nat. Commun.* **4**, 2171 (2013).
23. Sugden, S. M., Bego, M. G., Pham, T. N. & Cohen, E. A. Remodeling of the host cell plasma membrane by HIV-1 Nef and Vpu: a strategy to ensure viral fitness and persistence. *Viruses* **8**, 67 (2016).
24. van 't Wout, A. B. et al. Nef induces multiple genes involved in cholesterol synthesis and uptake in human immunodeficiency virus type 1-infected T cells. *J. Virol.* **79**, 10053–10058 (2005).
25. Rusinova, I. et al. Interferomev2.0: an updated database of annotated interferon-regulated genes. *Nucleic Acids Res.* **41**, D1040–D1046 (2013).

26. McLaren, P. J. et al. Identification of potential HIV restriction factors by combining evolutionary genomic signatures with functional analyses. *Retrovirology* **12**, 41 (2015).
27. Kosiol, C. et al. Patterns of positive selection in six mammalian genomes. *PLoS Genet.* **4**, e1000144 (2008).
28. Cohen, G. B. et al. The selective downregulation of class I major histocompatibility complex proteins by HIV-1 protects HIV-infected cells from NK cells. *Immunity* **10**, 661–671 (1999).
29. Zahoor, M. A. et al. HIV-1 Vpr induces interferon-stimulated genes in human monocyte-derived macrophages. *PLoS ONE* **9**, e106418 (2014).
30. Maitra, R. K. & Silverman, R. H. Regulation of human immunodeficiency virus replication by 2′,5′-oligoadenylate-dependent RNase L. *J. Virol.* **72**, 1146–1152 (1998).
31. Shah, A. H. et al. Degranulation of natural killer cells following interaction with HIV-1-infected cells is hindered by downmodulation of NTB-A by Vpu. *Cell Host Microbe* **8**, 397–409 (2010).
32. Grover, J. R., Veatch, S. L. & Ono, A. Basic motifs target PSGL-1, CD43, and CD44 to plasma membrane sites where HIV-1 assembles. *J. Virol.* **89**, 454–467 (2015).
33. Mangeat, B. et al. HIV-1 Vpu neutralizes the antiviral factor tetherin/BST-2 by binding it and directing its β-TrCP2-dependent degradation. *PLoS Pathog.* **5**, e1000574 (2009).
34. Margottin, F. et al. A novel human WD protein, h-βTrCp, that interacts with HIV-1 Vpu connects CD4 to the ER degradation pathway through an F-box motif. *Mol. Cell* **1**, 565–574 (1998).
35. Shirogane, T., Jin, J., Ang, X. L. & Harper, J. W. $SCF^{\beta\text{-}TrCP}$ controls clock-dependent transcription via casein kinase 1-dependent degradation of the mammalian period-1 (Per1) protein. *J. Biol. Chem.* **280**, 26863–26872 (2005).
36. Vigan, R. & Neil, S. J. Determinants of tetherin antagonism in the transmembrane domain of the human immunodeficiency virus type 1 Vpu protein. *J. Virol.* **84**, 12958–12970 (2010).
37. Cavrois, M., De Noronha, C. & Greene, W. C. A sensitive and specific enzyme-based assay detecting HIV-1 virion fusion in primary T lymphocytes. *Nat. Biotechnol.* **20**, 1151–1154 (2002).
38. Wu, Y., Beddall, M. H. & Marsh, J. W. Rev-dependent indicator T cell line. *Curr. HIV Res.* **5**, 394–402 (2007).
39. Lam, S. S. et al. Directed evolution of APEX2 for electron microscopy and proximity labeling. *Nat. Methods* **12**, 51–54 (2015).
40. Lamsoul, I., Uttenweiler-Joseph, S., Moog-Lutz, C. & Lutz, P. G. Cullin 5-RING E3 ubiquitin ligases, new therapeutic targets? *Biochimie* **122**, 339–347 (2016).
41. Sauter, D. & Kirchhoff, F. Multilayered and versatile inhibition of cellular antiviral factors by HIV and SIV accessory proteins. *Cytokine Growth Factor Rev.* **40**, 3–12 (2018).
42. Hotter, D. & Kirchhoff, F. Interferons and beyond: induction of antiretroviral restriction factors. *J. Leukoc. Biol.* **103**, 465–477 (2018).
43. Rihn, S. J. et al. The envelope gene of transmitted HIV-1 resists a late interferon γ-induced block. *J. Virol.* **91**, e02254-16 (2017).
44. Zhang, Y. et al. A robust error model for iTRAQ quantification reveals divergent signaling between oncogenic FLT3 mutants in acute myeloid leukemia. *Mol. Cell. Proteomics* **9**, 780–790 (2010).
45. Jiang, C. et al. A non-viral CRISPR/Cas9 delivery system for therapeutically targeting HBV DNA and pcsk9 in vivo. *Cell Res.* **27**, 440–443 (2017).
46. Roesch, F. et al. Hyperthermia stimulates HIV-1 replication. *PLoS Pathog.* **8**, e1002792 (2012).
47. Butler, S. L., Hansen, M. S. & Bushman, F. D. A quantitative assay for HIV DNA integration in vivo. *Nat. Med.* **7**, 631–634 (2001).
48. Martell, J. D., Deerinck, T. J., Lam, S. S., Ellisman, M. H. & Ting, A. Y. Electron microscopy using the genetically encoded APEX2 tag in cultured mammalian cells. *Nat. Protoc.* **12**, 1792–1816 (2017).

Acknowledgements

This work was supported by grants from the State Key Research Development Program of China to X.T. (no. 2016YFC1200303) and F.Z. (no. 2017YFA0505100), the China National Funds for Excellent Young Scientists (no. 31722030), grants from the National Natural Science Foundation of China to X.-F.Y. (no. 81772169) and F.Z. (no. 31670836), a grant from the Shanghai Institute of Higher Learning to F.Z. (no. TP2015003) and a grant from the NIMH, US Public Health Service to Y.W. (no. 5R01MH102144). We thank Q. Wang and X. Ye (Institute of Microbiology of the Chinese Academy of Sciences) for the use of the Biosafety level 3 Tissue Culture Facility. We thank H. Qi, N. Yan, H. Deng, A. Elia and N. Zheng for critical reading of the manuscript.

Author contributions

X.T. conceived and supervised the project. F.Z. conducted the mass spectrometry experiment and data analysis. Y.L. conducted most of the experiments with help from C.F., H.Z., S.L., T.Z. and X.K. Y.F., Z.Z. and D.D. conducted experiments on PSGL-1-blocking viral infectivity and western blot detection of PSGL-1 in virions. Y.W. supervised experiments on PSGL-1-blocking viral infectivity. J.Su and X.-F.Y. contributed to supervision and data analysis of the project. J.Sun and Y.Z. contributed key reagents and performed clinical analysis of the study. Q.W., J.G., M.L., W.Z. and Z.S. contributed to the data analysis. X.T. and F.Z. wrote and Y.W. edited the manuscript.

Competing interests

The authors declare no competing interests.

Additional information

Supplementary information is available for this paper at https://doi.org/10.1038/s41564-019-0372-2.

Reprints and permissions information is available at www.nature.com/reprints.

Correspondence and requests for materials should be addressed to F.Z., Y.W. or X.T.

Publisher's note: Springer Nature remains neutral with regard to jurisdictional claims in published maps and institutional affiliations.

nature research

Corresponding author(s): Xu Tan

Last updated by author(s): Dec 27, 2018

Reporting Summary

Nature Research wishes to improve the reproducibility of the work that we publish. This form provides structure for consistency and transparency in reporting. For further information on Nature Research policies, see Authors & Referees and the Editorial Policy Checklist.

Statistics

For all statistical analyses, confirm that the following items are present in the figure legend, table legend, main text, or Methods section.

n/a	Confirmed	
☐	☒	The exact sample size (*n*) for each experimental group/condition, given as a discrete number and unit of measurement
☐	☒	A statement on whether measurements were taken from distinct samples or whether the same sample was measured repeatedly
☐	☒	The statistical test(s) used AND whether they are one- or two-sided *Only common tests should be described solely by name; describe more complex techniques in the Methods section.*
☒	☐	A description of all covariates tested
☐	☒	A description of any assumptions or corrections, such as tests of normality and adjustment for multiple comparisons
☐	☒	A full description of the statistical parameters including central tendency (e.g. means) or other basic estimates (e.g. regression coefficient) AND variation (e.g. standard deviation) or associated estimates of uncertainty (e.g. confidence intervals)
☐	☒	For null hypothesis testing, the test statistic (e.g. *F*, *t*, *r*) with confidence intervals, effect sizes, degrees of freedom and *P* value noted *Give P values as exact values whenever suitable.*
☒	☐	For Bayesian analysis, information on the choice of priors and Markov chain Monte Carlo settings
☒	☐	For hierarchical and complex designs, identification of the appropriate level for tests and full reporting of outcomes
☐	☒	Estimates of effect sizes (e.g. Cohen's *d*, Pearson's *r*), indicating how they were calculated

Our web collection on statistics for biologists contains articles on many of the points above.

Software and code

Policy information about availability of computer code

Data collection	BD LSR Fortessa SORP BD FACS Aria SORP Olympus IX83 FV1200 Thermo ARRAYSCAN VTI HCS Reader Bio-Rad CFX96 Real-Time System FluorChem FC3
Data analysis	GraphPad Prism 6.0 ImagJ 1.5 FlowJo2 Imaris9 Bio-Rad CFX Maestro

For manuscripts utilizing custom algorithms or software that are central to the research but not yet described in published literature, software must be made available to editors/reviewers. We strongly encourage code deposition in a community repository (e.g. GitHub). See the Nature Research guidelines for submitting code & software for further information.

Data

Policy information about availability of data

All manuscripts must include a data availability statement. This statement should provide the following information, where applicable:

- Accession codes, unique identifiers, or web links for publicly available datasets
- A list of figures that have associated raw data
- A description of any restrictions on data availability

All data generated or analysed during this study are included in this published article and supplementary information file.

Field-specific reporting

Please select the one below that is the best fit for your research. If you are not sure, read the appropriate sections before making your selection.

☒ Life sciences ☐ Behavioural & social sciences ☐ Ecological, evolutionary & environmental sciences

For a reference copy of the document with all sections, see nature.com/documents/nr-reporting-summary-flat.pdf

Life sciences study design

All studies must disclose on these points even when the disclosure is negative.

Sample size	Each QPCRs and FACs experiment has been performed at least 3 times (n ≥3) and each n has at least 2 technical repeats. Blot analyses were performed at least twice.
Data exclusions	No data were excluded.
Replication	Each QPCRs and FACs experiment has been performed at least 3 times(n ≥3) and each n has at least 2 technical repeats. Blot analyses were performed at least twice.
Randomization	No randomization was performed.
Blinding	No blinding was performed.

Reporting for specific materials, systems and methods

We require information from authors about some types of materials, experimental systems and methods used in many studies. Here, indicate whether each material, system or method listed is relevant to your study. If you are not sure if a list item applies to your research, read the appropriate section before selecting a response.

Materials & experimental systems

n/a	Involved in the study
☐	☒ Antibodies
☐	☒ Eukaryotic cell lines
☒	☐ Palaeontology
☒	☐ Animals and other organisms
☐	☒ Human research participants
☒	☐ Clinical data

Methods

n/a	Involved in the study
☒	☐ ChIP-seq
☐	☒ Flow cytometry
☒	☐ MRI-based neuroimaging

Antibodies

Antibodies used	The information of all antibodies used are described in the manuscript.
Validation	All antibodies used have been validated.

Eukaryotic cell lines

Policy information about cell lines

Cell line source(s)	Jurkat cells E6.1 clone, MAGI-CCR5 cells, TZM-bl cells were from NIH HEK293T cells were from ATCC Rev-A3R5-GFP cells were from Virongy.
Authentication	Cells were checked permanently according to morphology and function features or resistant to certain antibiotics.
Mycoplasma contamination	Cell lines have been regularly test for mycoplasma contamination using a commercial kit (Vazyme). If contaminated, cells would be discarded.
Commonly misidentified lines (See ICLAC register)	No commonly misidentified cell lines were used.

Human research participants

Policy information about studies involving human research participants

Population characteristics	The healthy participants were in the age range 16-40.
Recruitment	Volunteer participants were selected based on two criteria: (1) they are HIV negative; (2) they are in good health condition.
Ethics oversight	The study has been approved by the Institutional Review Board of Beijing You'An Hospital.

Note that full information on the approval of the study protocol must also be provided in the manuscript.

Flow Cytometry

Plots

Confirm that:

☒ The axis labels state the marker and fluorochrome used (e.g. CD4-FITC).

☒ The axis scales are clearly visible. Include numbers along axes only for bottom left plot of group (a 'group' is an analysis of identical markers).

☒ All plots are contour plots with outliers or pseudocolor plots.

☒ A numerical value for number of cells or percentage (with statistics) is provided.

Methodology

Sample preparation	The preparation processes of cell fixation and staining are described in manuscript.
Instrument	Data were collected on BD LSR Fortessa SORP and different cell population were separated by BD FACS Aria SORP.
Software	FlowJo2
Cell population abundance	The abundance were identified by using control groups like isotope staining or uninfected cell group.
Gating strategy	Gated only high forward/side scatter cells to ensure exclusion of cell debris.

☒ Tick this box to confirm that a figure exemplifying the gating strategy is provided in the Supplementary Information.